



Calhoun: The NPS Institutional Archive
DSpace Repository

Theses and Dissertations

1. Thesis and Dissertation Collection, all items

2005-06

High energy solid state and free electron laser systems in tactical aviation

Mansfield, Robb P.

Monterey, California. Naval Postgraduate School

<http://hdl.handle.net/10945/1922>

Downloaded from NPS Archive: Calhoun



Calhoun is the Naval Postgraduate School's public access digital repository for research materials and institutional publications created by the NPS community. Calhoun is named for Professor of Mathematics Guy K. Calhoun, NPS's first appointed -- and published -- scholarly author.

Dudley Knox Library / Naval Postgraduate School
411 Dyer Road / 1 University Circle
Monterey, California USA 93943

<http://www.nps.edu/library>



NAVAL POSTGRADUATE SCHOOL

MONTEREY, CALIFORNIA

THESIS

**HIGH ENERGY SOLID STATE AND FREE ELECTRON
LASER SYSTEMS IN TACTICAL AVIATION**

by

Robb P. Mansfield

June 2005

Thesis Advisor:
Second Reader:

William B. Colson
Robert L. Armstead

Approved for public release; distribution is unlimited

THIS PAGE INTENTIONALLY LEFT BLANK

REPORT DOCUMENTATION PAGE			<i>Form Approved OMB No. 0704-0188</i>	
Public reporting burden for this collection of information is estimated to average 1 hour per response, including the time for reviewing instruction, searching existing data sources, gathering and maintaining the data needed, and completing and reviewing the collection of information. Send comments regarding this burden estimate or any other aspect of this collection of information, including suggestions for reducing this burden, to Washington headquarters Services, Directorate for Information Operations and Reports, 1215 Jefferson Davis Highway, Suite 1204, Arlington, VA 22202-4302, and to the Office of Management and Budget, Paperwork Reduction Project (0704-0188) Washington DC 20503.				
1. AGENCY USE ONLY (Leave blank)		2. REPORT DATE June 2005	3. REPORT TYPE AND DATES COVERED Master's Thesis	
4. TITLE AND SUBTITLE: High Energy Solid State and Free Electron Laser Systems in Tactical Aviation			5. FUNDING NUMBERS	
6. AUTHOR(S) Major Robb P. Mansfield, USMC				
7. PERFORMING ORGANIZATION NAME(S) AND ADDRESS(ES) Naval Postgraduate School Monterey, CA 93943-5000			8. PERFORMING ORGANIZATION REPORT NUMBER	
9. SPONSORING /MONITORING AGENCY NAME(S) AND ADDRESS(ES) N/A			10. SPONSORING/MONITORING AGENCY REPORT NUMBER	
11. SUPPLEMENTARY NOTES The views expressed in this thesis are those of the author and do not reflect the official policy or position of the Department of Defense or the U.S. Government.				
12a. DISTRIBUTION / AVAILABILITY STATEMENT Approved for public release; distribution is unlimited.			12b. DISTRIBUTION CODE A	
13. ABSTRACT (maximum 200 words) A study and analysis of high energy laser (HEL) systems aboard tactical aircraft is performed. The FA-18E/F Hornet and F-35 Joint Strike Fighter (JSF), equipped with solid-state HEL systems, are the main subjects of the study. Considerations of power generation and thermal management for a fighter-sized HEL system and aero-optic effects on beam propagation from high and medium altitude platforms are examined. An overview of system capabilities details how the HEL system will be more difficult to incorporate into legacy strike aircraft, but may be feasible for future aircraft such as the JSF. Tactical flight simulations are used to study and develop potential concepts of operation (CONOPS), using realistic scenarios and threat environments. Results show that a tactical HEL will not be a stand-alone weapon in combat, but will have many potentially useful tactical applications. Another study of a high energy free electron laser (FEL) system aboard C-130J-30 Hercules shows that such a system is feasible. Finally, a study of the FEL shows that strong field extraction can be optimized using undulator tapering.				
14. SUBJECT TERMS Solid State Laser, Free Electron Laser, Directed Energy, High Energy Laser, Tactical Aircraft, HEL, FEL, SSL, C-130J-30, Joint Strike Fighter, FA-18E/F, Hornet, F-35, Fiber Laser, High Power Laser			15. NUMBER OF PAGES 100	
			16. PRICE CODE	
17. SECURITY CLASSIFICATION OF REPORT Unclassified	18. SECURITY CLASSIFICATION OF THIS PAGE Unclassified	19. SECURITY CLASSIFICATION OF ABSTRACT Unclassified	20. LIMITATION OF ABSTRACT UL	

THIS PAGE INTENTIONALLY LEFT BLANK

Approved for public release; distribution is unlimited

**HIGH ENERGY SOLID STATE AND FREE ELECTRON LASER SYSTEMS IN
TACTICAL AVIATION**

Robb P. Mansfield
Major, United States Marine Corps
B.S., Rensselaer Polytechnic Institute, 1993

Submitted in partial fulfillment of the
requirements for the degree of

MASTER OF SCIENCE IN APPLIED PHYSICS

from the

**NAVAL POSTGRADUATE SCHOOL
June 2005**

Author: Robb P. Mansfield

Approved by: William B. Colson
Thesis Advisor

Robert L. Armstead
Second Reader

James H. Luscombe
Chairman, Department of Physics

THIS PAGE INTENTIONALLY LEFT BLANK

ABSTRACT

A study and analysis of high energy laser (HEL) systems aboard tactical aircraft is performed. The FA-18E/F Hornet and F-35 Joint Strike Fighter (JSF), equipped with solid-state HEL systems, are the main subjects of the study. Considerations of power generation and thermal management for a fighter-sized HEL system and aero-optic effects on beam propagation from high and medium altitude platforms are examined. An overview of system capabilities details how the HEL system will be more difficult to incorporate into legacy strike aircraft, but may be feasible for future aircraft such as the JSF. Tactical flight simulations are used to study and develop potential concepts of operation (CONOPS), using realistic scenarios and threat environments. Results show that a tactical HEL will not be a stand-alone weapon in combat, but will have many potentially useful tactical applications. Another study of a high energy free electron laser (FEL) system aboard a C-130J-30 Hercules shows that such a system is feasible. Finally, a study of the FEL shows that strong field extraction can be optimized using undulator tapering.

THIS PAGE INTENTIONALLY LEFT BLANK

TABLE OF CONTENTS

I.	SOLID STATE LASER (SSL) THEORY	1
A.	INTRODUCTION.....	1
B.	CONCEPT EVOLUTION.....	1
C.	STIMULATED EMISSION.....	2
D.	PUMPING SCHEMES.....	3
	1. Population Inversion.....	3
	2. Pumping	6
	3. Pumping Processes.....	8
E.	OPTICAL RESONATORS.....	10
	1. Longitudinal and Transverse Modes of the Cavity	11
	2. Cavity Q	13
F.	CURRENT SOLID STATE LASER TECHNOLOGY.....	14
	1. Diode Pump Efficiency for High Power Solid State Lasers	14
	2. High Power Fiber Lasers.....	16
	3. Tunable Solid-State Lasers	19
II.	HIGH ENERGY SOLID-STATE LASER TACTICAL AIR EMPLOYMENT CONCEPT	21
A.	PLATFORMS AND INTEGRATION.....	21
	1. FA-18E/F Super Hornet	21
	2. F-35 Joint Strike Fighter (JSF).....	22
	3. MV-22 Osprey	23
B.	HEL FIGHTER SIMULATION	24
C.	POTENTIAL ROLES AND MISSIONS	26
	1. Air-to-Ground	27
	a. <i>Target Types and Vulnerabilities</i>	27
	b. <i>Close Air Support (CAS)</i>	30
	c. <i>Air Interdiction</i>	32
	d. <i>Suppression of Enemy Air Defenses (SEAD)</i>	34
	e. <i>Surface-to-Air Missile (SAM) Defense</i>	36
	2. Air-to-Air	36
	a. <i>Offensive Counter Air (OCA) / Defensive Counter Air (DCA)</i>	37
	b. <i>Air Combat Maneuvering (ACM)</i>	38
D.	PERFORMANCE CONSIDERATIONS.....	39
	1. Power Generation	39
	a. <i>Joint Strike Fighter</i>	39
	b. <i>FA-18E/F</i>	40
	2. Thermodynamics.....	43
	a. <i>Thermal Management of the Lasing Medium</i>	45

	<i>b. Thermal Management of Surrounding Airframe Components</i>	46
	3. Aero-Optic Effects	47
	<i>a. Turbulence</i>	48
	<i>b. Absorption and Scattering</i>	51
E.	CONCLUSIONS	56
III.	THE FREE ELECTRON LASER AS A TACTICAL AIRBORNE WEAPON..	59
A.	CONCEPT EVOLUTION.....	59
B.	FEL COMPONENTS	59
C.	PROPERTIES OF FEL SYSTEMS.....	61
D.	FREE ELECTRON LASER INTEGRATION INTO TACTICAL AIRBORNE PLATFORMS.....	62
	1. C-130J-30 Constraints.....	62
	2. Integration Considerations	63
	3. 350 kW FEL Parameters.....	64
	4. Simulation Results	65
IV.	FEL THEORY	69
A.	FUNDAMENTAL EQUATIONS.....	69
	1. Lorentz Equations.....	69
	2. Undulator and Optical Field Strengths.....	69
B.	ELECTRON MOTION IN THE UNDULATOR	70
C.	ELECTRON MOTION IN THE OPTICAL FIELD.....	71
D.	PHASE SPACE	73
E.	THE ELECTRON BEAM IN PHASE SPACE.....	74
V.	FEL UNDULATOR TAPER SIMULATION	77
A.	UNDULATOR TAPER	77
B.	SIMULATION RESULTS	77
	LIST OF REFERENCES.....	79
	INITIAL DISTRIBUTION LIST	83

LIST OF FIGURES

Figure 1.	Components of the Ruby Laser	2
Figure 2.	Stimulated Emission Process	3
Figure 3.	Energy Level Population Diagram.....	5
Figure 4.	Three-level pumping	7
Figure 5.	Four-level pumping.....	8
Figure 6.	Absorption Spectrum of Nd:YAG	9
Figure 7.	Semiconductor Diode Laser and Bandgap Diagram.....	10
Figure 8.	Optical Resonator of a Solid State Laser	11
Figure 9.	Single-Cladding Fiber Laser	16
Figure 10.	Cladding-Pumped Scheme.....	18
Figure 11.	HEL-equipped FA-18E/F.....	22
Figure 12.	F-35 HEL concept.....	23
Figure 13.	MV-22 HEL integration.....	24
Figure 14.	Instrument Panel Display of HEL simulator.....	25
Figure 15.	Heads-Up Display of HEL simulator.....	25
Figure 16.	HEL simulator target data.....	26
Figure 17.	Daytime Low-Threat CAS for HEL-equipped aircraft.....	31
Figure 18.	HEL employment for Air Interdiction mission.....	33
Figure 19.	HEL fighter SEAD scenario	35
Figure 20.	Air Intercept Scenario	38
Figure 21.	RAT generator concept.....	43
Figure 22.	Notional Heat Flow Concept for FA-18E/F.....	47
Figure 23.	Turbulence Effects on Transverse Intensity	50
Figure 24.	Beam Spreading Effect of Moderate Turbulence for Co-Altitude Shot	51
Figure 25.	Atmospheric Transmission Windows at Sea Level	53
Figure 26.	Plot of Power on Target vs. Altitude for Air-to-Ground Scenario	54
Figure 27.	Plot of Power on Target vs. Altitude for Air-to-Air Scenario	55
Figure 28.	Plot of Power on Target vs. Range for Air-to-Air Scenario	56
Figure 29.	Basic Components of an FEL System	60
Figure 30.	C-130J-30 General Specifications	62
Figure 31.	350 kW Airborne FEL Layout Concept.....	65
Figure 32.	Optical Mode Shape of 350 kW FEL design	66
Figure 33.	Electron-Photon Race	73
Figure 34.	Electrons in Closed Orbit Phase Space Trajectories.....	74
Figure 35.	End State Phase Space of Electrons.....	75
Figure 36.	FEL Undulator Taper Rate vs. Strong Field Extraction	78

THIS PAGE INTENTIONALLY LEFT BLANK

LIST OF TABLES

Table 1.	Typical Efficiencies of Diode-Pumped Laser Systems	15
Table 2.	Required Power on Target for Common Target Materials	29
Table 3.	Comparison of HEL and conventionally equipped strike fighter in the low and medium threat CAS role.....	31
Table 4.	Maximum Ranges of Common SAM systems.....	34
Table 5.	C_n^2 Values for Different Turbulence Models.....	48
Table 6.	350 kW FEL Simulation Parameters	64
Table 7.	350 kW FEL Simulation Results	66

THIS PAGE INTENTIONALLY LEFT BLANK

ACKNOWLEDGEMENTS

In writing this thesis, I received help and information from a great many people. First and foremost, I would like to thank my wife Mary. Her support and guidance was invaluable, and made it possible for me to complete what I hope she finds to be a meaningful work. Of course, my two wonderful children, Dane and Maeve, gave me plenty of support, each in their own way.

In my endeavor, I was fortunate to have an inspirational and highly knowledgeable advisor, Dr. William Colson. His expertise in the field of high energy laser physics as well as his ability to effectively teach the principles of such things to a Marine made the process of thesis writing a great learning experience for me. Additionally, I was fortunate to be part of the Free Electron Laser research group here at NPS and the other professors in the group were also great sources of help and knowledge: Dr. Joseph Blau, Dr. Robert Armstead, and Dr. Peter Crooker.

Much of my tactics study was done at the Naval Air Systems Command Warfare Analysis Department in Patuxent River, MD. Specifically, Mr. Carlos Falcon, Ms. Nancy Gould, and Ms. Anuradha Simlote were all extremely helpful, and I look forward to continuing to work with them in the future.

Ms. Michelle Creedon at Northrop Grumman Space Technology went out of her way to help me, and provided me with some great information. I extend many thanks to her and the other professionals at NGST.

Dr. Roy Whitney and Dr. George Neil at Jefferson Laboratory assisted me with Free Electron Laser integration concepts, and for that I thank them.

Despite the many people who helped me along the way, everything contained in this thesis is my own work, and thus any mistakes in facts or conclusions can be only attributed to me.

THIS PAGE INTENTIONALLY LEFT BLANK

I. SOLID STATE LASER (SSL) THEORY

A. INTRODUCTION

The limits of current technology preclude some types of lasers from being used aboard tactical, fighter-sized aircraft. Chemical lasers, which function by mixing two or more chemicals to produce laser energy, are bulky and contain hazardous materials not suitable for tactical aviation or the shipboard environment of the aircraft carrier. Free-Electron lasers, which are described in section V, operating at short wavelengths require a long (10 m) accelerator that cannot fit within the limited space available on a fighter-sized aircraft. This primarily leaves solid state lasers as the only option for producing weapon-quality laser radiation for these platforms. There are still many physics issues that arise from designing such a system, and these will be discussed at length in section II.C.

B. CONCEPT EVOLUTION

On May 16, 1960, the first laser was operated at the Hughes Laboratory in Culver City, California¹. This laser was a solid state laser, with a ruby crystal 1 cm in diameter and 1.5 cm long as the lasing medium. This “first light” did not actually produce a visible spot, but rather the lasing was verified by a change in the fluorescence spectrum of the ruby crystal. Later the flash lamp power was increased, and the laser spot became visible.

The predecessor of the laser was the maser, Microwave Amplification by the Stimulated Emission of Radiation. The maser idea started in the early 1950s, and was mainly pushed along by scientists in the Soviet Union². The basic idea of the maser was a resonant cavity through which a molecular beam of excited molecules was fired. These molecules (the first was a beam of ammonia molecules) produced microwave radiation at

¹ Townes, C. H., How The Laser Happened, p. 104, Oxford University Press, 1999

² Townes, p. 63

approximately right angles to the beam as the de-excitation of the molecular states occurred. The resonant cavity allowed the microwaves to further amplify incoming molecules to higher energy states, while some microwaves were emitted from the cavity as maser radiation. The first maser was successfully fired at Columbia University in early April 1954³.

The maser gave new life to the idea of stimulated emission, thus leading the way for the laser. The basic configuration of the first solid state laser was an intense flash lamp coiled around a ruby crystal inside a resonant chamber. The flash lamp was the mechanism for optical pumping (described in section I.D), and thus the initiation of stimulated emission. In this case, the resonant chamber was a set of mirrors, one of which was almost completely reflective, and the other was partially reflective in order to release the laser radiation. Figure 1 below shows the basic design of the first ruby laser.

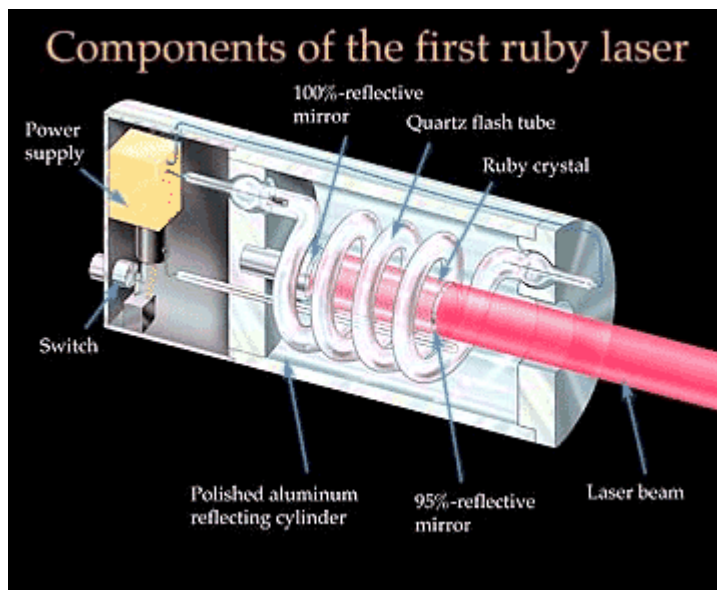


Figure 1. Components of the Ruby Laser⁴

C. STIMULATED EMISSION

Spontaneous emission of radiation occurs when an atom or molecule transitions from an excited energy state to a lower energy state without any external stimulation.

³ Townes, p. 66

⁴ Extracted from <http://www.llnl.gov/nif/library/aboutlasers/how.html>

Stimulated emission, however, occurs when excited atoms are pumped by an external source and are “forced” into a lower energy state in the presence of radiation, thus emitting radiation energy.

The principle of stimulated emission is the essence of the laser, and it was first hypothesized by Albert Einstein in 1917. He used the principle of detailed balance, which states in general terms that in thermodynamic equilibrium, the rate of any process must be exactly balanced by the rate of the corresponding reverse process ⁵. Thus in stimulated emission processes for lasers, electrons of atoms undergo a transition to a lower energy state stimulated by an incoming photon, and the net result is two outgoing photons of the same phase, frequency, and direction. That, is the net result is monochromatic, coherent light. Figure 2 shows an illustration of stimulated emission. The incoming photon has energy $E = \hbar\omega$, where \hbar is Planck’s constant divided by 2π , and ω is the photon angular frequency. This energy is the same as the difference between energy levels of the atom, $\Delta E = E_2 - E_1$. Two coherent photons emerge at angular frequency ω , with total energy $E = 2\hbar\omega$.

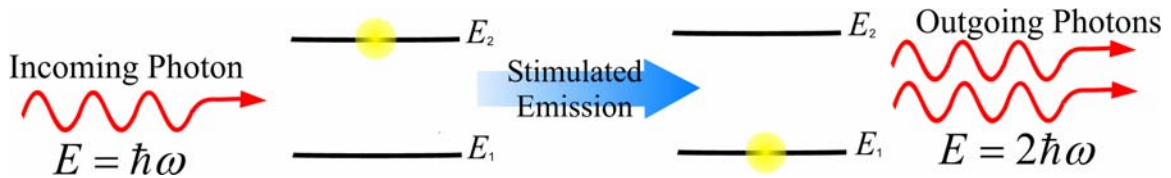


Figure 2. Stimulated Emission Process

D. PUMPING SCHEMES

1. Population Inversion

To achieve lasing action in a solid-state laser, stimulated emission must be accompanied by the condition of population inversion. Population inversion, simply stated, is the condition where the number of atoms with excited energy levels outnumber

⁵ Svelto, O., Principles of Lasers, 4th ed., Plenum Press, New York and London, 1998

that of the ground state. Boltzmann's Principle states that in thermal equilibrium (at temperature T in Kelvin), the populations of any two energy levels are given by ⁶

$$\frac{N_2}{N_1} = \exp\left(-\frac{E_2 - E_1}{k_B T}\right) \quad (1)$$

where N_1 and N_2 are the populations of energy levels 1 and 2, E_1 and E_2 are the energies of those levels, k_B is the Boltzmann constant, and T is the temperature in Kelvin. Thus, for atoms in thermal equilibrium, the higher energy level population is always smaller than the lower level population (i.e. $N_2 < N_1$), since T is positive, and $E_2 > E_1$. Therefore, the stimulated emission rate (from the upper level) will always be less than that of the absorption rate (by the lower level). The principle of detailed balance holds that

$$AN_2 + B_{21}\rho N_2 = B_{12}\rho N_1, \quad (2)$$

where A , B_{12} , and B_{21} are the Einstein coefficients (determined by the nature of the particular transition), ρ is the photon density, and N_1 and N_2 are the populations of energy levels 1 and 2. Note that only the stimulated transitions depend on the photon density since spontaneous emission is independent of any existing light. Figure 3 shows an energy level population diagram, illustrating the spontaneous emission and stimulated transitions of Equation(2).

⁶ Siegman, A., Lasers, University Science Books, Sausalito, California, 1986

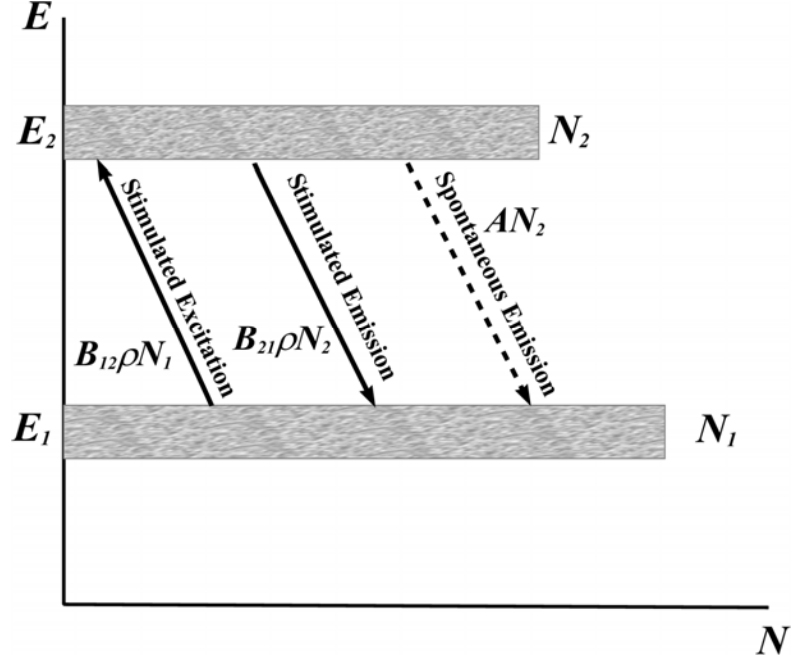


Figure 3. Energy Level Population Diagram

The first term in Equation (2), AN_2 represents the rate of spontaneous emission from the higher energy level 2 to level 1. The second term, $B_{21}\rho N_2$ represents the rate of stimulated emission from level 2 to level 1. The third term, $B_{12}\rho N_1$, represents the rate of excitation (or absorption) to level 2 from level 1 by incoming photons. Solving for the density of states yields

$$\rho = \frac{A/B_{12}}{N_1/N_2 - B_{21}/B_{12}} \quad (3)$$

The populations of each state are given by their Boltzmann distributions, and thus the ratio of their populations becomes

$$\frac{N_1}{N_2} = \frac{e^{-E_1/kT}}{e^{-E_2/kT}} = e^{\hbar\omega/kT}, \quad (4)$$

since $(E_2 - E_1) = \hbar\omega$ by Planck's Law.

The spectral energy density, or the density of photons at frequency ω for a certain temperature T , is given by Planck's Law for blackbody radiation⁷

⁷ Svelto, p. 23

$$\rho(\omega) = \frac{2\pi\hbar\omega^2}{\pi c^3 (e^{\hbar\omega/kT} - 1)} \quad (5)$$

Inserting Equation (3) into (4) and Equating to (5) yields

$$\rho = \frac{A/B_{12}}{e^{\hbar\omega/kT} - B_{21}/B_{12}} = \frac{\frac{2\hbar\omega^2}{\pi c^3}}{e^{\hbar\omega/kT} - 1} \quad (6)$$

In thermal equilibrium, $B_{21} = B_{12}$, and so $A/B = 2\hbar\omega^2 / \pi c^3$.

Thus, the ratio of probability of spontaneous emission to that of stimulated emission is given by

$$\frac{A}{B\rho} = e^{\frac{\hbar\omega}{kT}} - 1 \quad (7)$$

It can be seen from Equation (7) that for $\hbar\omega \ll kT$ (e.g., visible light at room temperature), spontaneous emission (represented by the Einstein A coefficient) is the dominant process. For $\hbar\omega \gg kT$ (e.g. visible light inside a star), stimulated emission (represented by the B coefficient) is the dominant process.

2. Pumping

To overcome the dominance of spontaneous emission over stimulated emission under normal conditions requires a process known as "pumping", by which energy is added to the system so that a population inversion ($N_2 > N_1$) exists. The process of pumping elevates electrons to a metastable state, which has a relatively long decay time and creates the population inversion necessary for lasing. The nonradiative transition of this higher energy state is blocked by the size of the energy gap to the next lower state⁸, and so the stimulation of this level from an incoming photon causes a radiative transition.

A two-energy level system would not work for lasing simply because the population inversion could not be maintained. Once the atoms are excited to the higher energy level, the probability of further stimulated emission and absorption are equal, and

⁸ Siegman, p.17

the condition of saturation occurs, and no population inversion can exist⁹. Therefore, solid-state lasers are either three- or four-level systems. In a three-level system, shown in Figure 3, pumping occurs between the ground state, E_0 , and E_2 , the upper energy state. The rapid, nonradiative decay occurs between E_2 and E_1 , the metastable state. The stimulated, radiative transition then occurs between E_1 and E_0 . Note that the population N_1 of E_1 is greater than that of the ground state. Thus the population inversion, and laser transition, in this case occurs between level 1 and the ground state.

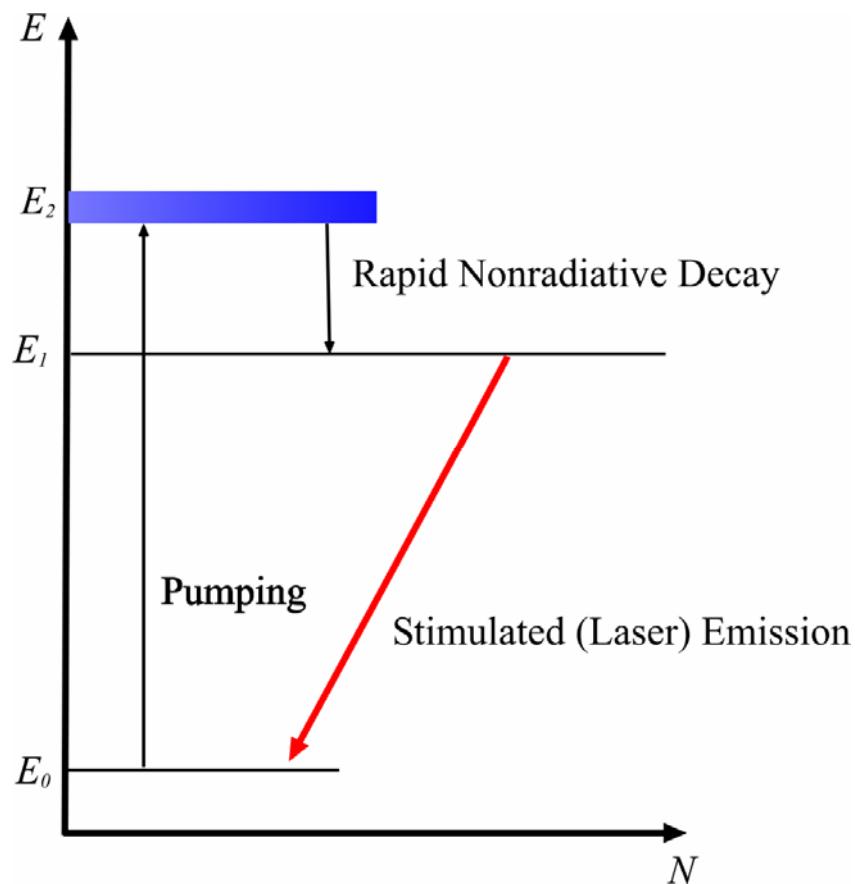


Figure 4. Three-level pumping

Similarly, a four-level pumping scheme (as shown in Figure 4) has a population inversion between E_2 (the metastable state) and E_1 . The pumping requirements of a four-level system are typically much smaller than those of three-level systems. Since the energy gap $E_1 - E_0$ is much greater than the

⁹ Svelto, p. 61

thermal energy of operation, kT , the populations of levels 1, 2, and 3 will be much smaller than the population of the ground state (by equation (1)). When atoms are pumped from the ground state to level 3, and then a rapid nonradiative process brings them to the metastable state, a population inversion quickly develops, since the E_1 state is relatively unpopulated.

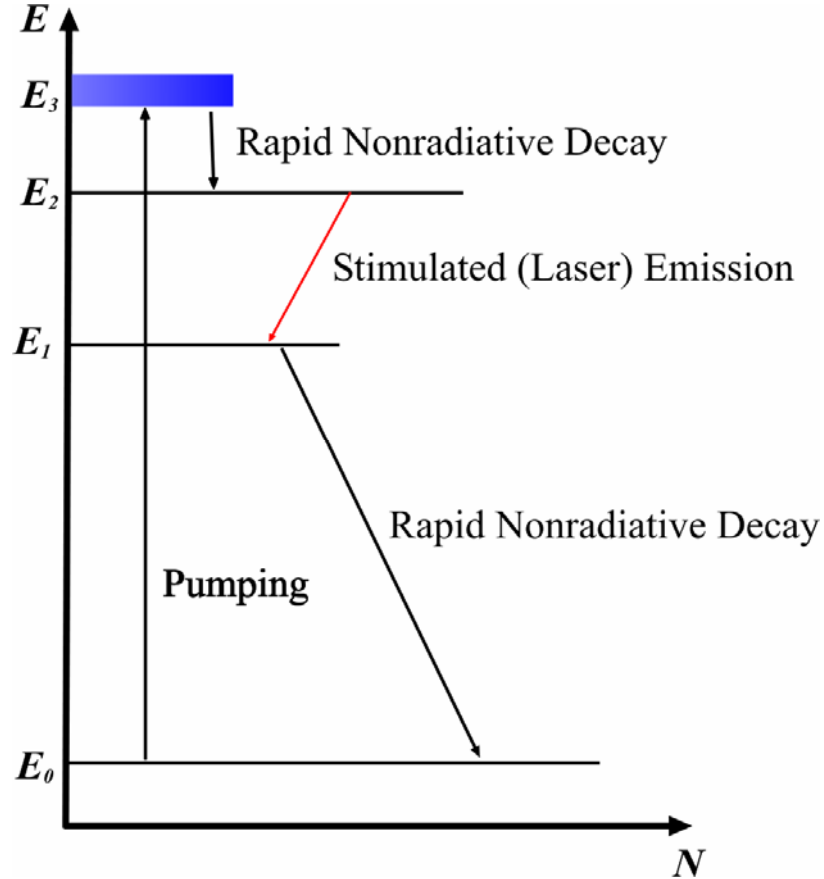


Figure 5. Four-level pumping

3. Pumping Processes

There are two primary pumping methods used to achieve a population inversion. The ruby laser used optical pumping, by which incoherent, higher energy photons are fired into the lasing medium to excite the atoms. The ruby laser used a flash lamp to excite Cr^{3+} ions (grown as a 0.05% impurity in the crystal) at the appropriate wavelength. In this case, the bandwidth of the absorption lines was quite broad (as opposed to sharp lines), and so white light could be used. The blue and green lines were absorbed exciting

the atoms, and then a nonradiative transition occurred to two separate metastable states, followed by the laser transition.

Another optical pumping method is laser pumping. Since atoms with sharp absorption lines can absorb the monochromatic light of lasers, it is suitable for solid state, liquid and gaseous lasers. The most commonly used laser pumping method is diode pumping, using high-efficiency (around 50-60%) semiconductor diode lasers ¹⁰. An example of this is the Nd:YAG laser, which uses an AlGaAs pumping diode at a wavelength of 808nm. This wavelength is not the laser wavelength (1.06 μm), but rather the wavelength required to pump the atoms to the higher excited state. Figure 4 shows the absorption spectrum of the Nd:YAG laser.

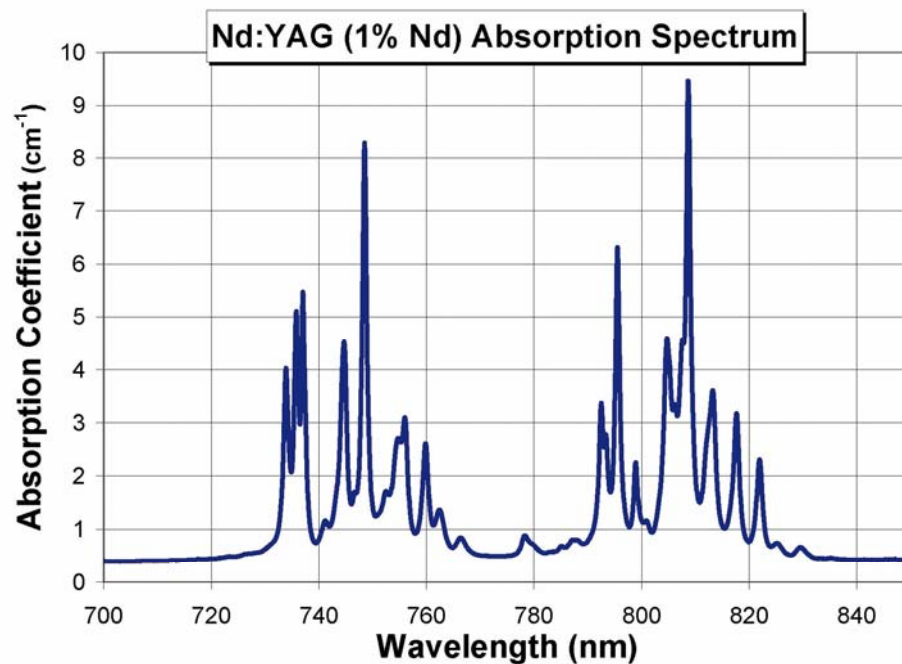


Figure 6. Absorption Spectrum of Nd:YAG ¹¹

¹⁰ Svelto, p. 201

¹¹ www.st.northropgrumman.com/synoptics/SiteFiles/docs/PDFs/Nd_YAG_graph.pdf

Another method of pumping is electrical pumping, in which an intense electrical discharge creates ions and free electrons that collide with the atoms of the lasing medium (a gas). In a semiconductor laser, such as those used for diode pumping, a forward voltage bias over a p-n junction is used to create a population inversion of electrons in the conduction band to holes in the valence band. Figure 6 shows a simple design of a semiconductor laser and the electrical pumping process for a semiconductor laser. The voltage bias puts electrons from the n-type material into the conduction band of the active medium, and holes from the p-type material into the valence band, thus creating a population inversion across the bandgap.

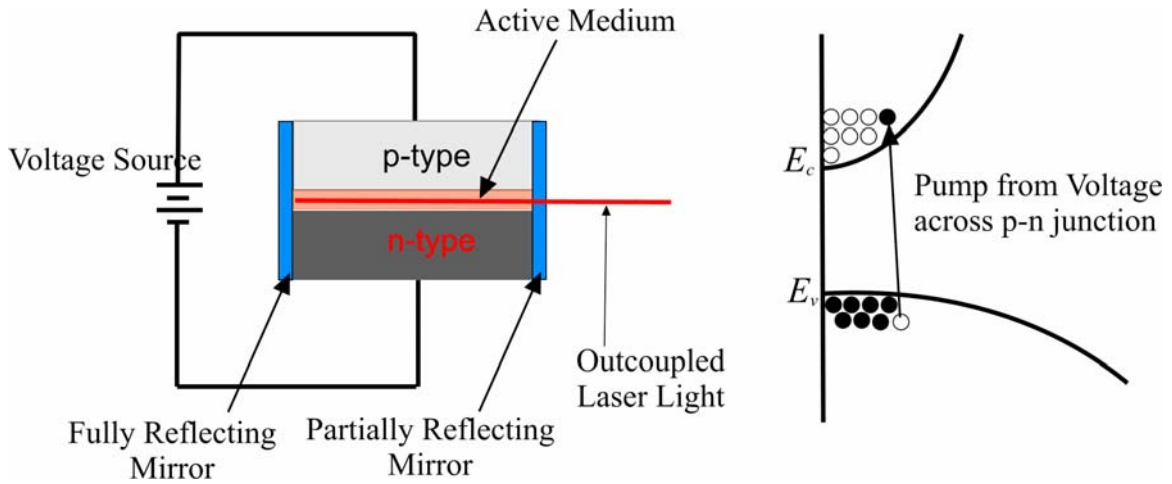


Figure 7. Semiconductor Diode Laser and Bandgap Diagram

E. OPTICAL RESONATORS

As the laser light of the active medium is emitted, it propagates along the axis of the resonator, and is reflected, at least partially, by the mirrors of the optical resonator. The reflected light provides additional stimulated emission as it passes through the active medium (again), since the photons are of the appropriately quantized energy, $E = \hbar\omega$, to stimulate emission from the pumped energy level. Eventually, the photons are transmitted, or outcoupled, by a partially reflecting mirror at one end of the cavity.

Typically, the mirrors of the optical resonator are slightly spherically concave, and circular in shape. The typical length of the resonator (for a lower power laser), L , is between a few centimeters and 1 m, and the mirror dimensions do not usually exceed a few centimeters ¹². This is not always the case, however, especially in high power applications, which will be discussed in detail in later sections. Figure 8 shows a typical laser resonator configuration.

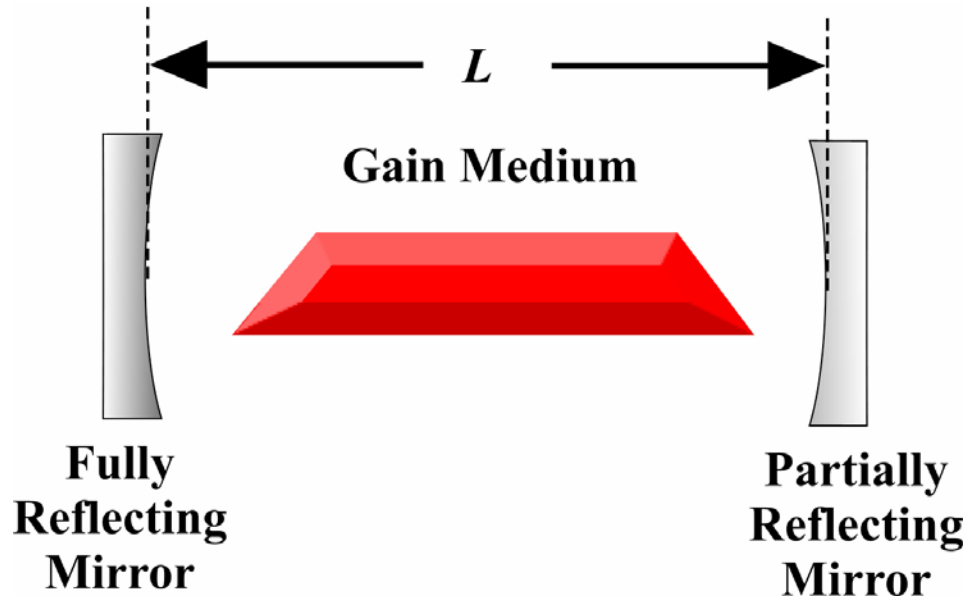


Figure 8. Optical Resonator of a Solid State Laser

1. Longitudinal and Transverse Modes of the Cavity

The cavity length determines the possible longitudinal modes of a laser cavity in a similar way to the length of a string determining the modes of the string. For a laser, only modes corresponding to half-wavelength multiples will survive, and other others will be attenuated. This is an important factor in determining the precise cavity length, such that

$$\frac{m\lambda}{2} = L \quad (8)$$

¹² Svelto, p. 161

where L is the cavity length and m is an integer (mode number). As an example, for a fighter-sized solid-state laser, $L=0.5\text{m}$ and laser wavelength $\lambda=1.06\mu\text{m}$, so that the fractional mode spacing allowed by the resonator is then $\Delta m/m \approx 10^{-6}$. A typical high power laser has a fractional linewidth of approximately 10^{-3} , and so they run in many modes. Most lasers run in many modes. Achieving a narrow spectrum is desirable for adequate beam propagation (discussed in section II.C.3), especially for weaponized lasers, which need to propagate over long distances through narrow transmission windows in the atmosphere.

From Equation (8) it follows that the frequency of each mode, ω_m , is given by

$$\omega_m = m \left(\frac{c}{2L} \right) \frac{1}{2\pi} \quad (9)$$

and so the frequency spacing between the longitudinal modes of the cavity becomes

$$\frac{\Delta\omega_m}{\Delta m} = \frac{c}{4\pi L} \quad (10)$$

The transverse modes of the cavity refer to the optical fields of the cavity over cross-sectional areas perpendicular to the axis of propagation¹³. As the light is bounced back and forth between the mirrors, it will diffract off-axis and thus spread out transversely. The fundamental mode of a cavity corresponds to a smooth distribution of light across the cavity in a Gaussian profile. It is essential for a laser to be operating in the fundamental transverse mode (also called the TEM₀₀ mode) for long distance, low diffraction, free space propagation¹⁴, as in the case for weaponized high power lasers. Note that this idealized fundamental mode shape is difficult to achieve when an active medium is present (e.g. in a solid-state laser). This modal dependence for beam propagation will be discussed further in section II.C.3.

¹³ Siegman, p. 43

¹⁴ Kuznetsov, M., Stern, M., Coppeta, J., "Single Transverse Mode Optical Resonators", *Optics Express*, Vol. 13, No. 1, 10 January 2005

2. Cavity Q

Laser cavities typically are open so that there are losses due to diffraction as energy leaks out to beyond the mirror edges, a phenomenon called “walk-off loss”¹⁵. Additionally, there are losses from resistive effects of the gain medium, and transmissive effects such as mirror absorption.

The non-diffraction related losses of a particular cavity can be quantified by its quality factor, or Q-factor. The number of photons $\phi(t_m)$ of a beam of initial intensity $I_0 \propto \phi_0$ propagating through a cavity after m round trips (at time t_m) is given by ¹⁶

$$\phi(t_m) = [R_1 R_2 (1 - T_i)^2]^m \phi_0, \quad (11)$$

where R_1 and R_2 are the reflectivities of the cavity mirrors, and T_i represents all the internal resistive losses. Over many passes, losses can be approximated by an exponential decay based on photon lifetime, τ_c ,

$$\phi(t_m) = \phi_0 \exp\left(\frac{-t_m}{\tau_c}\right) \quad (12)$$

Equating (11) and (12), and solving for the characteristic decay time τ_c yields:

$$\tau_c = \frac{L}{c\gamma_L}, \quad (13)$$

where $t_m = 2Lm/c$ is the time to make m round trips, and γ_L is the cavity loss,

$$\gamma_L = \frac{-2}{\ln[R_1 R_2 (1 - T_i)^2]}. \quad (14)$$

The quality factor Q is defined by

$$Q = \frac{2\pi \times (\text{energy stored})}{\text{energy lost in one oscillation cycle}} \quad (15)$$

¹⁵ Siegman, p. 43

¹⁶ Svelto, p.167

A high Q value relates to a resonant system with low losses. The energy stored in the system is equal to the number of photons times the photon energy, $\phi\hbar\omega$, and the energy lost in one oscillation cycle is equal to $-\hbar\frac{d\phi}{dt}$ ¹⁷. Therefore, from equations (12) and (15):

$$Q = -\frac{2\pi\omega\phi}{(d\phi/dt)} = 2\pi\omega\tau_c. \quad (16)$$

Thus there is a distinct proportionality of cavity Q to both frequency of operation and photon lifetime. The frequency spectrum (linewidth) $\Delta\nu_c$ of the emitted light is obtained from the Fourier transform of the field power and is given by¹⁸

$$\Delta\nu_c = \frac{1}{2\pi\tau_c} \quad (17)$$

Combining (16) and (17), the Q of the cavity can then be written as

$$Q = \frac{\nu}{\Delta\nu_c} \quad (18)$$

F. CURRENT SOLID STATE LASER TECHNOLOGY

1. Diode Pump Efficiency for High Power Solid State Lasers

Solid state laser (SSL) systems deployed on tactical aircraft will likely rely on the efficiency and size of diode pumps (as described in section I.D.3.) to achieve lasing action. Recently, high-average-power solid state lasers, specifically neodymium and ytterbium doped yttrium aluminum garnet (Nd:YAG and Yb:YAG) have been shown to produce pump absorption efficiencies (i.e. [light absorbed at the pumping frequency]/[diode laser light into the medium]) of around $\eta_a \approx 80\%$ ¹⁹. As a comparison, typical

¹⁷ Svelto, p. 169

¹⁸ Svelto, p. 169

¹⁹ Bass, M. Dong, J. "Properties of Diode Laser Pumps for High-Power Solid State Lasers", *IEEE Journal of Quantum Electronics*, Vol. 41, No.2, February 2005

absorption efficiency for a lamp-pumped Nd-YAG laser is approximately 17%, and the absorption efficiency of the lamp-pumped ruby laser is about 28% ²⁰.

The system efficiency η_s of a high power solid state laser system is critical to its feasibility for a fighter-sized aircraft, since the prime power available will be severely limited. The overall efficiencies of some common lasers are shown below in Table 1 ²¹. Note that the efficiencies listed do not include any required subsystems, such as a cooling system, and only represent the efficiencies of the lasers themselves.

Table 1. Typical Efficiencies of Diode-Pumped Laser Systems

Laser Type	η_s (%)
1.064 μm Nd:YAG	18
1.064 μm Nd: Glass	14
1.064 μm Nd: BeL	12

The pump efficiency η_p can be quantified as follows ²²

$$\eta_p = \eta_r \eta_t \eta_a \eta_{pq} \quad (19)$$

where η_r is the pumping lamp (or diode laser) efficiency ([power out] / [power into lamp]), η_t is the transfer efficiency ([power entering the medium] / [power emitted by lamp at the pump wavelength]), and η_{pq} is the power quantum efficiency (fraction of absorbed power actually used to populate the upper laser energy level).

The system efficiency η_s ([power into laser]/[power out in the laser beam]) of a system can be calculated as follows ²³

$$\eta_s = \eta_p \eta_c \eta_q \eta_t \quad (20)$$

²⁰ Svelto, p. 210

²¹ Koechner, W. Solid State Laser Engineering, 5th ed., Springer, 1999, p.137

²² Svelto, p. 209

²³ Svelto, p. 261

where η_c is the fraction of generated photons that are outcoupled (outcoupling efficiency), η_q is the fraction of minimum pump energy transformed into laser energy (laser quantum efficiency), and η_t is the fraction of lasing medium cross section to the optical beam cross section (transverse efficiency).

As can be seen in Table 1, the efficiency of a 1 W Nd:YAG laser is around 18%. The goal efficiency of high power solid-state lasers under development is approximately 10%²⁴. Thus, a 50 kW laser would require approximately 500 kW of power from the aircraft, with most of the excess 450 kW power appearing as heat. This will be discussed further in section II.C.

2. High Power Fiber Lasers

Due to their potential for compact size, high output power, and high system efficiencies, fiber lasers may be the preferred design for high power solid state laser systems aboard tactical aircraft. A fiber laser typically consists of a single mode core (i.e. only allows the fundamental mode) doped with the desired laser ion (e.g. ytterbium, neodymium), surrounded by cladding. Nd:Glass and Yb:Glass are types of lasing media typically used in fiber lasers. Figure 10 shows a schematic of a single-cladding fiber laser.

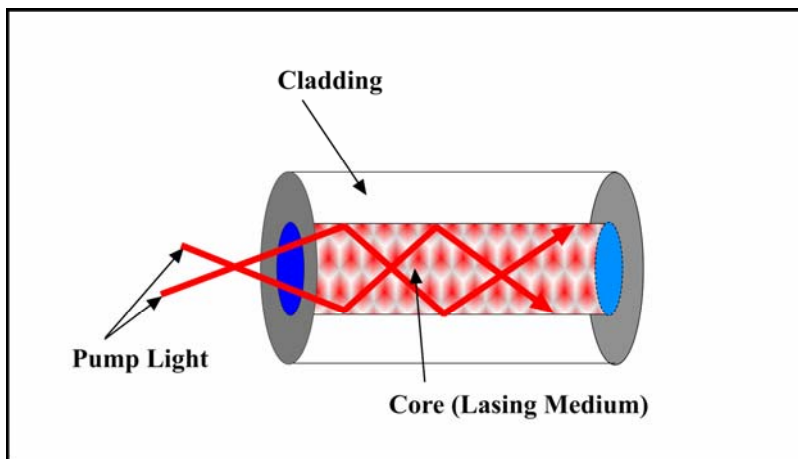


Figure 9. Single-Cladding Fiber Laser

²⁴ Erwin, S. "Tactical Laser Weapons Still Many Years Away", *National Defense*, August 2002

Traditional, lower power fiber lasers are end-pumped with laser diode light. However, the higher power laser diodes by nature contain many transverse modes, and thus tend to produce lower beam quality²⁵, called M^2 . The beam quality M^2 is a comparison of the transverse mode of the actual beam to the ideal Gaussian (fundamental) mode. That is, it quantifies the content of higher order modes and can be expressed as ²⁶

$$M^2 = \left(\frac{W}{w} \right)^2, \quad (21)$$

where W is the transverse extent of the beam (including all modes), and w is the transverse extent of the ideal Gaussian mode. An ideal, perfect Gaussian beam would have an $M^2 = 1$, and would have optimum propagation characteristics, as will be discussed in section II. C. In contrast, a badly distorted beam would have $M^2 > 50$.

To compensate for this lower beam quality in high power diode pumps, the fiber laser is “cladding-pumped”. This requires a double-cladded fiber, with the inner cladding having refractive index n_i and the outer cladding having refractive index n_o such that $n_o < n_i < n_{core}$. Diode pump light enters the inner cladding, as shown in Figure 11, and as it undergoes internal reflection through the fiber, only the fundamental mode is absorbed by the single mode core.

²⁵ Gapontsev, V., Krupke, W., “Fiber Lasers Grow in Power”, *Laser Focus World*, August 2002, pp. 83-87

²⁶ Hall, D. R., Jackson, P. E., The Physics and Technology of Laser Resonators, IOP Publishing, New York, NY, 1989, p.133

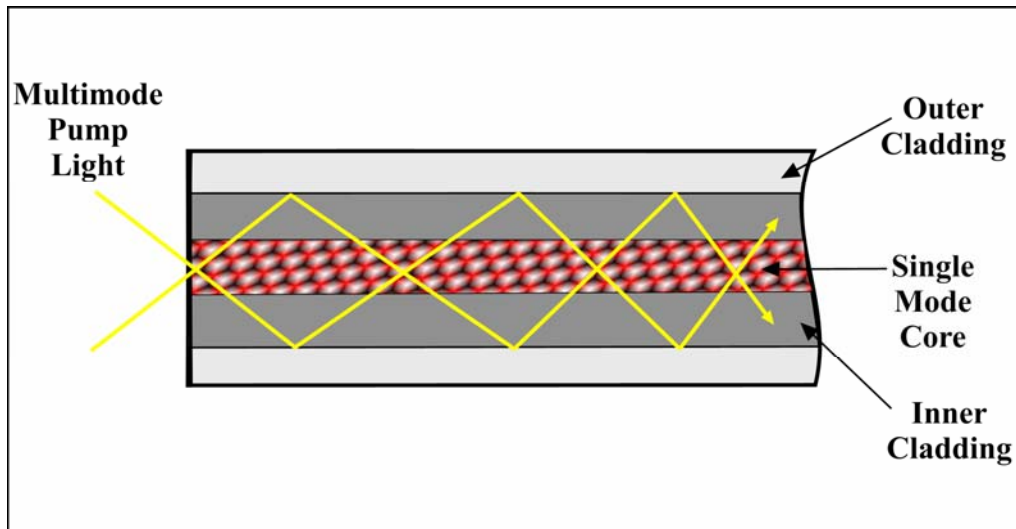


Figure 10. Cladding-Pumped Scheme

A type of fiber laser called a large mode area (LMA) laser has made it possible to produce diffraction-limited (i.e. good beam quality) powers up to twice that of conventional solid-state lasers like the Nd:YAG ²⁷. LMA fibers use larger cross-sectional cores, and can thus have thicker claddings for cladding-pumping. LMA fibers of beam quality of $M^2 = 1.24$ have been built, and advanced designs of LMA fibers may be able to produce 10kW from a single fiber²⁸.

To produce a high power (>25 kW) laser for an airborne system may require a phased array of such fibers. The coherent addition of laser energy is a challenge, as the exact phase matching of each beam must occur. However, a highly efficient combination of four fiber lasers has been achieved ²⁹, and it is likely that further advances will be made.

Another potentially promising technology is the area of photonic crystal fiber lasers (PCFL). PCFLs use shorter fiber lengths, thus requiring higher absorption efficiencies. These shorter fiber lengths could potentially achieve high powers while avoiding or reducing detrimental nonlinear effects such as Brillouin and Raman

²⁷ Galvanauskas, A., "High Power Fiber Lasers", *Optics and Photonics News*, July 2004

²⁸ Galvanauskas

²⁹ Shirakawa, A. Saitou, T., Sekiguchi, T., Ueda, K., "Coherent addition of fiber lasers by use of a fiber coupler", *Optics Express*, Vol 10 No. 21, October 2002

scattering ³⁰. Additionally, photonic crystal fibers have holes on the order of 1 μm to effectively reduce the refractive index of the core. These holes run parallel to the axis of the fiber and could possibly be used to flow coolant, air or otherwise, through the lasing medium in order to dissipate heat. Thermal management will be discussed in section II. C.

Lastly, the coiling of fibers is not only a feasible option for reducing space requirements, but is also a technique to remove higher-order modes, and thus improve beam quality. The fiber curvature induces a refractive index slope, which allows the higher-order modes to escape into the cladding ³¹.

3. Tunable Solid-State Lasers

One disadvantage of most solid state lasers is that they are not wavelength-tunable. Tunable solid-state lasers, such as the alexandrite laser and the titanium sapphire laser, have demonstrated power levels of 0.1 kW ³². Unfortunately, the wavelength regimes of available tunable solid state systems do not fall within good atmospheric transmission windows, and so the weapon utility of such lasers is limited.

³⁰ Mifi, A., Moloney, J., Kouznetsov, D., Schulzgen, A., Jiang, S., Luo, T., Peyghambarian, N., "A Large-Core Compact High-Power Single-Mode Photonic Crystal Fiber Laser", *IEEE Photonics Technology Letters*, Vol 16 No. 12, December 2004

³¹ Galvanauskas

³² Svelto, p. 381

THIS PAGE LEFT INTENTIONALLY BLANK

II. HIGH ENERGY SOLID-STATE LASER TACTICAL AIR EMPLOYMENT CONCEPT

A. PLATFORMS AND INTEGRATION

This research was conducted using models of the FA-18E/F Super Hornet and the F-35 Joint Strike Fighter (JSF). However, the scope of research being conducted is by no means limited to those two platforms. HEL integration is being studied for numerous other types of aircraft, including both fixed and rotor-wing.

In addition to integration engineering considerations of an HEL system aboard a naval strike aircraft, there exist many issues specific to HEL aircraft aboard U.S. Navy aircraft carriers. They must be resistant to potential exposure to salt water (sea spray), as well as hardened to the numerous carrier catapult takeoffs and arrested landings which put a severe strain on aircraft systems and components. The maintenance of the system must be able to be performed aboard the ship while underway, with minimal excess equipment.

1. FA-18E/F Super Hornet

Integration of a HEL system into the FA-18E/F is a challenge. The physics of the major technical considerations will be discussed in section II.C. Since the FA-18E/F airframe is already filled to capacity with avionics and other systems, the HEL system would need to be externally mounted, perhaps in a centerline-mounted pod in order to maximize the downward field-of-view (FOV) of the system. Additionally, a power generation and/or storage unit, which will likely be required on the Super Hornet, will be externally mounted on station 4 or station 8 (see figure 12 below). Figure 12 shows a concept picture of the FA-18E/F with an onboard HEL system.



Figure 11. HEL-equipped FA-18E/F

2. F-35 Joint Strike Fighter (JSF)

The JSF may be more suited to HEL integration, as far as the power requirement is concerned. The most optimum placement of the HEL into the JSF may be into the fan bay, which would contain the lift fan for the Short Takeoff and Vertical Landing (STOVL) variant of the F-35. The driveshaft for the lift fan, which is capable of producing nearly 1 MW of mechanical power, could be coupled to a high-efficiency generator to produce power for the onboard laser. The approximately 100-cubic foot bay could house the generator and HEL system, and the laser light could be outcoupled via mirrors to a beam director on either the top or bottom of the aircraft, depending on the target location. Figure 13 shows a concept schematic for the HEL integration into the JSF³³.

³³ Burris, T. K., "Directed Energy - Worth Analysis and Vehicle Evaluation (DE-WAVE): Military Utility of High-Energy Laser (HEL) Fighter", AFRL-VA-WP-TR-2003-3082, Lockheed Martin Aeronautics Company, Raytheon Company, Physical Sciences, Inc, Air Force Research Laboratory (AFRL), August 2003

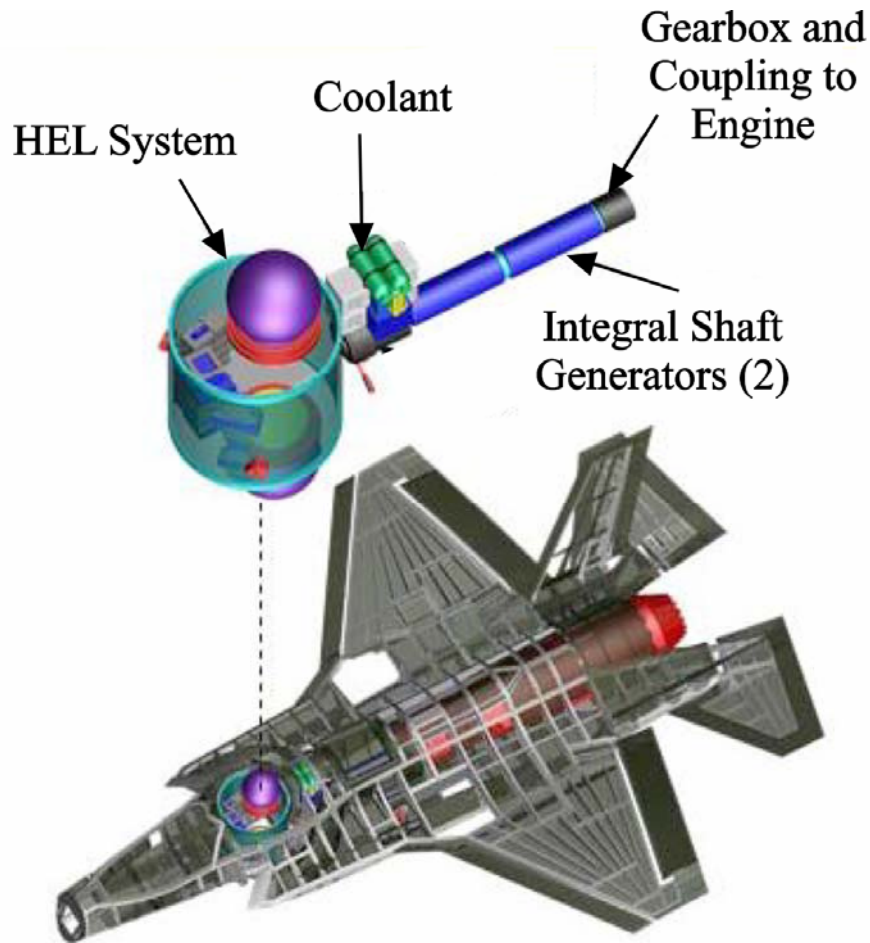


Figure 12. F-35 HEL concept

3. MV-22 Osprey

While not strictly classified as a tactical strike aircraft, the MV-22 Osprey may provide the most suitable platform for solid state HEL integration. The MV-22 will be designed to have 736 cubic feet of usable internal cargo space, as well as a combat payload of 20,000 lbs. This would allow for a larger, more powerful HEL system, as well as accompanying generators, capacitors, and cooling subsystems to fit within the cargo area of the Osprey. Laser light could be outcoupled to either side of the aircraft to maximize field-of-regard and even to attack two targets simultaneously by using a beam splitter. Figure 13 shows a simplified concept diagram for HEL integration into the MV-22 Osprey.

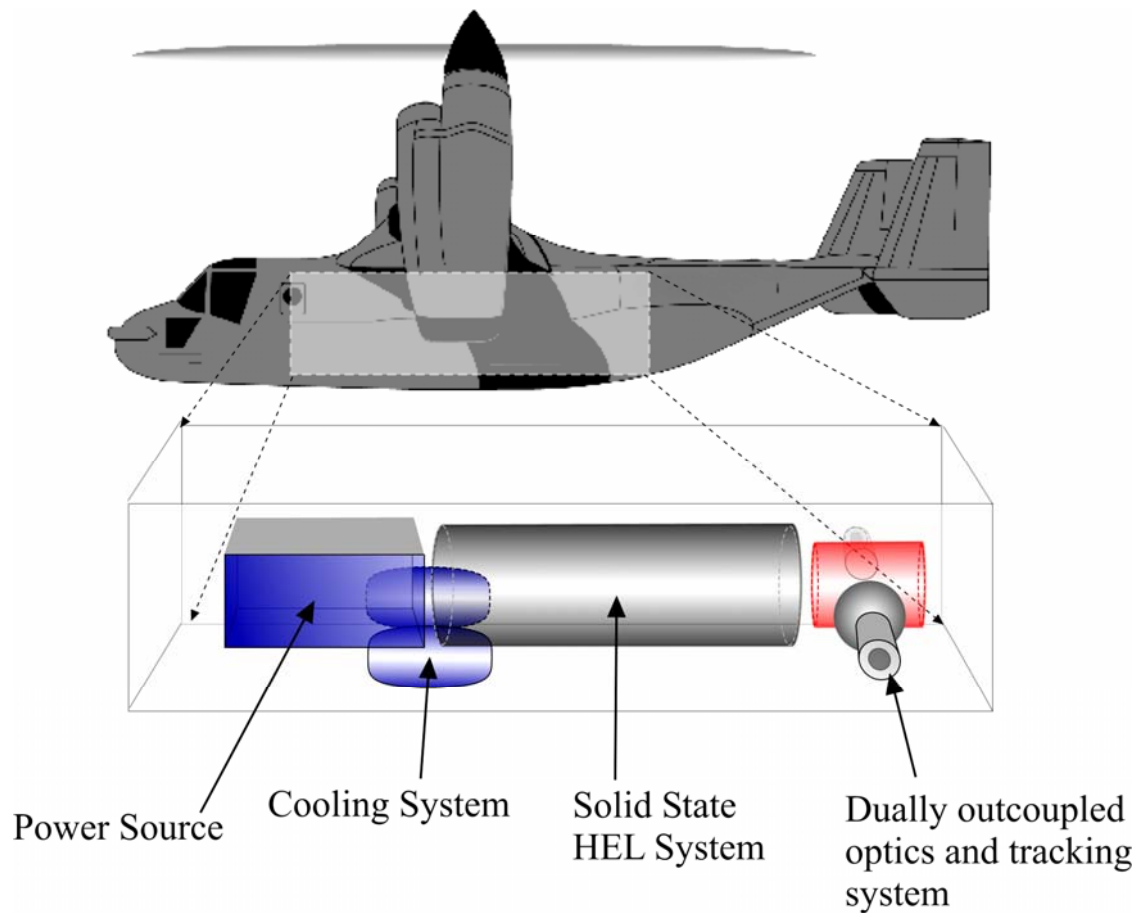


Figure 13. MV-22 HEL integration

B. HEL FIGHTER SIMULATION

To develop and evaluate potential tactics for an HEL-equipped strike fighter, simulations were performed (flown), using the HEL mini-crew station simulators at the Air Combat Test and Evaluation Facility (ACETEF) at Naval Air Station, Patuxent River, MD. The ACETEF mini-crew stations incorporate the cockpit environment of the FA-18E Super Hornet into a realtime simulation of tactical scenarios. Missions can be flown against air, land and sea targets, and data can be recorded and stored for later analysis.

Air-to-air, as well as air-to-ground simulations were performed using current tactical doctrine. The simulations were also performed using non-standard tactics to evaluate possible advantages of the HEL in certain scenarios. Figures 14 and 15 show the two cockpit views of the simulator.



Figure 14. Instrument Panel Display of HEL simulator

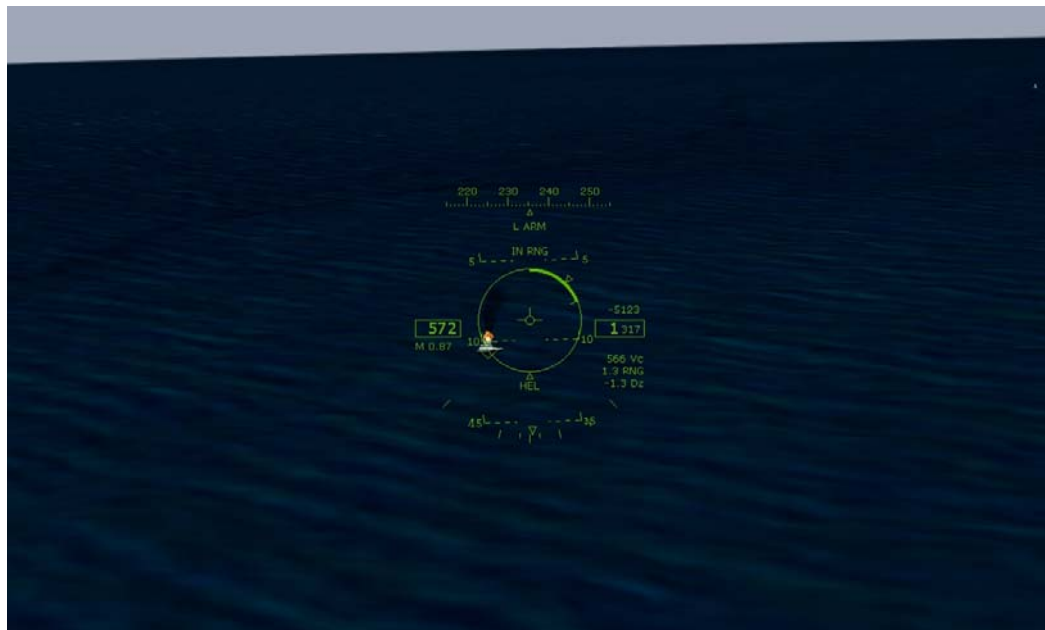


Figure 15. Heads-Up Display of HEL simulator

In Figure 14, the display on the far left-hand side is the FLIR display, where targeting and aimpoint selection for the HEL is performed. The other displays, as well as

the Heads-Up Display in Figure 15, are similar to those that are in the FA-18E/F. Figure 16 shows the target data collected from one simulated attack on a light armored vehicle.



Figure 16. HEL simulator target data

In the figure, the laser aimpoint is depicted by a red dot, and the laser intensity at the target, shot range, and pulse duration are shown in the lower left corner.

C. POTENTIAL ROLES AND MISSIONS

The roles and missions of an HEL-equipped strike fighter will likely complement those of conventionally-armed aircraft and ground forces, and though there may be unique missions for which an HEL is suited, it will not be an area-effect weapon, or “bunker buster”, capable of delivering catastrophic damage to hardened targets. More likely, it will be used to minimize collateral damage around soft targets (light vehicles, radar sites, etc.), destroy and/or immobilize multiple soft targets, or defend against incoming threat missiles. “Combined arms” is defined as the “full integration of arms in such a way that in order to counteract one, the enemy must make himself more vulnerable to another...”³⁴ The following is a qualitative professional supposition on potential missions and tactics which may exploit the HEL in both the autonomous and combined arms roles, based on experience and thorough the simulations performed at the Air Combat Environment Test and Evaluation Facility at Naval Air Station Pax River, MD (as described in the previous section).

³⁴ Marine Corps Doctrinal Publication 1 (MCDP 1) Warfighting, Headquarters, U.S. Marine Corps, 1997

1. Air-to-Ground

The air-to-ground role has been the primary wartime role of the naval strike fighter since the first flight of the FA-18 Hornet in November 1978³⁵, which served as a replacement for both the F-4 Phantom (fighter) and A-7 Corsair II (attack) in the US Navy and Marine Corps. Undoubtedly, an HEL system could have many roles in the air-to-ground environment, many of which will only be discovered and developed after an HEL system has been fielded.

a. Target Types and Vulnerabilities

A big limitation to the utility of the HEL in the air-to-ground arena will be the target types that it can be used against. However, there will be some targets, and some target locations for which the HEL will be optimum.

The amount of material that a HEL can ablate, or destroy, is determined primarily by the fluence on the target (total energy delivered per unit area), the dwell time on targets, and the material properties of the target, namely the heat capacity and melting point. For simplicity, the reflectivity of materials is not a factor, since the surface of the target material will likely be blackened (i.e. near zero reflectivity) almost immediately. The intensity, Φ , on the target is defined as

$$\Phi = \frac{P_t}{A} \quad (22)$$

where P_t is the laser beam power on the target, and A is the cross-sectional area of the beam spot on the target.

The laser beam spot radius $w(z)$ at a range z , assuming plane wave propagation, is given by³⁶

³⁵ <http://www.history.navy.mil/planes/fa18.htm>

³⁶ Svelto, p. 151

$$w(z) = \sqrt{w_0^2 \left[1 + \left(\frac{\lambda z}{\pi w_0^2} \right)^2 \right]}, \quad (23)$$

where w_0 is the beam waist radius at $z=0$, and λ is the laser wavelength. For $z \ll w_0^2$, equation (23) becomes

$$w \approx \frac{\lambda z}{\pi w_0} \quad (24)$$

Now, if the minimum beam waist, is assumed to be at the target at range Z (i.e. ideally focused), then

$$w_s = \frac{\lambda Z}{\pi w(Z)}, \quad (25)$$

where $w(Z)$ is the beam radius at the exit aperture, and w_s is the laser beam spot radius.

The fluence F on target is obtained from the time integral of the intensity

$$F = \int_0^\tau \Phi dt = \frac{P_t \tau}{A} = \frac{P_t \tau}{\pi (w_0)^2} = \frac{P_t \tau \pi r_a^2}{\lambda^2 z^2} \quad (26)$$

where τ is the time the laser is on the target, or “dwell time”, and $r_a = w(Z)$ is the aperture radius at the laser beam director.

The required fluence on a particular target, and thus the lethality of the HEL with respect to that target, is determined by the amount of energy needed to ablate enough material to cause sufficient damage to the target. For example, ablation of 10 cubic centimeters of material on a radar dish may not effectively disable it, but ablating the same amount of material on the nosecone of a missile traveling at Mach 3.0 may bring about catastrophic aerodynamic instability which would tear the missile apart.

The energy required to effectively kill a target is given by the product of the mass of the material times the heat per unit mass to reach melting temperature plus the heat per unit mass to melt. This approach assumes that no significant heat is removed by thermal conduction or convection. The heat per unit mass to reach melting temperature depends on the specific heat of the material, so that

$$Q_k = A\rho d \left[C_v (T_m - T_0) + \Delta H_m \right], \quad (27)$$

where ρ is the material density, d is the thickness of the material, C_v is the specific heat, T_m is the melting temperature of the material, T_0 is the temperature of the material, and ΔH_m is the heat of melting per unit mass. Thus, the fluence (energy per unit area) to “kill” a target is

$$F_k = \frac{Q_k}{A} = \rho d \left[C_v (T_m - T_0) + \Delta H_m \right]. \quad (28)$$

Equating (23) to (27), and solving for P_t yields

$$P_t = \frac{\lambda^2 z^2}{\pi \tau r_a^2} \rho d \left[C_v (T_m - T_0) + \Delta H_m \right], \quad (29)$$

which is the required power on target for an effective kill. Table 2 below shows some common target materials for air-to-ground scenarios, and the power required to kill the target. For the data below, range Z is 5 nautical miles (nm), τ is 4 seconds (a nominal dwell time), the beam director radius r_a is 0.3 meters, and λ is 1.06 microns.

Table 2. Required Power on Target for Common Target Materials

Target	Target Material	ρ (g / cm ³)	d (cm)	C_v (J / (g °K))	ΔH_m (J / g)	T_m (K)	T_0 (K)	P_t (kW)
Air Search Radar Dish	Aluminum Alloy	2.71	10.0	0.91	321	932	300	22.1
SAM nosecone	Ceramic*	3.0	1.0	0.9	1600	3300	250	12.1
T-72 Tank Armor	Steel**	7.85	10.0	0.5	272	2327	300	93.8
Light Armored Vehicle skin	Titanium Carbide (TiC) Ceramic	5.1	2.0	0.72	3000	2765	300	45.3
* Average value for carbon-carbon ceramic matrix types								
** Average value for all steel types								

Note that the values obtained for P_t in Table 2 are those required to ablate a certain depth (d) of material, and may not represent the intensity (power/spot size)

required to effectively destroy the target. This would depend on the particular scenario, i.e. a high speed missile may only require a 1 cm² area ablated to cause a catastrophic aerodynamic failure, while a radar antenna for a SAM site may require a larger area to effectively destroy it. Additionally, equation (29) does not account for atmospheric losses, turbulence, or target reflectivity (i.e. all the incident energy is assumed to be absorbed).

b. Close Air Support (CAS)

The Close Air Support (CAS) mission is defined as “Air action by fixed- and rotary-wing aircraft against hostile targets that are in close proximity to friendly forces and that require detailed integration of each air mission with the fire and movement of those forces”³⁷. One of the primary concerns in any CAS mission is the direction and proximity of friendly forces, due to possible collateral effects from conventional high explosive ordnance. It is possible that with a laser weapon, the rules-of-engagement (ROE) for CAS aircraft could be expanded to beyond that currently allowed. That is, CAS aircraft could strike targets much closer to friendly troops, even intermingled with friendly troops, given that positive identification has been established by some means.

CAS aircraft are controlled by a Forward Air Controller (FAC), either on the ground or in the air (FAC (A)). There are three distinct types of CAS: high threat, medium threat, and low threat CAS ³⁸. In a high threat scenario, surface defenses are such that the CAS aircraft must fly a very low-altitude ingress. This would likely preclude the effective use of the HEL system, due to terrain masking until the very last seconds of the attack, and thus preclude the associated tracking system to acquire the target.

In medium and low-threat CAS, the aircraft are elevated to some preplanned altitude, and so have a better opportunity to acquire and track the target with

³⁷ Joint Publication 1-02 (JP 1-02), U.S. Department of Defense

³⁸ Marine Aviation Weapons and Tactics Squadron One (MAWTS -1) FAC(A) Handbook, January 2004

onboard systems, and thus employ an HEL weapon on the target. Figure 15 shows a notional geometry for a daytime, low-threat CAS scenario for two HEL-equipped aircraft.

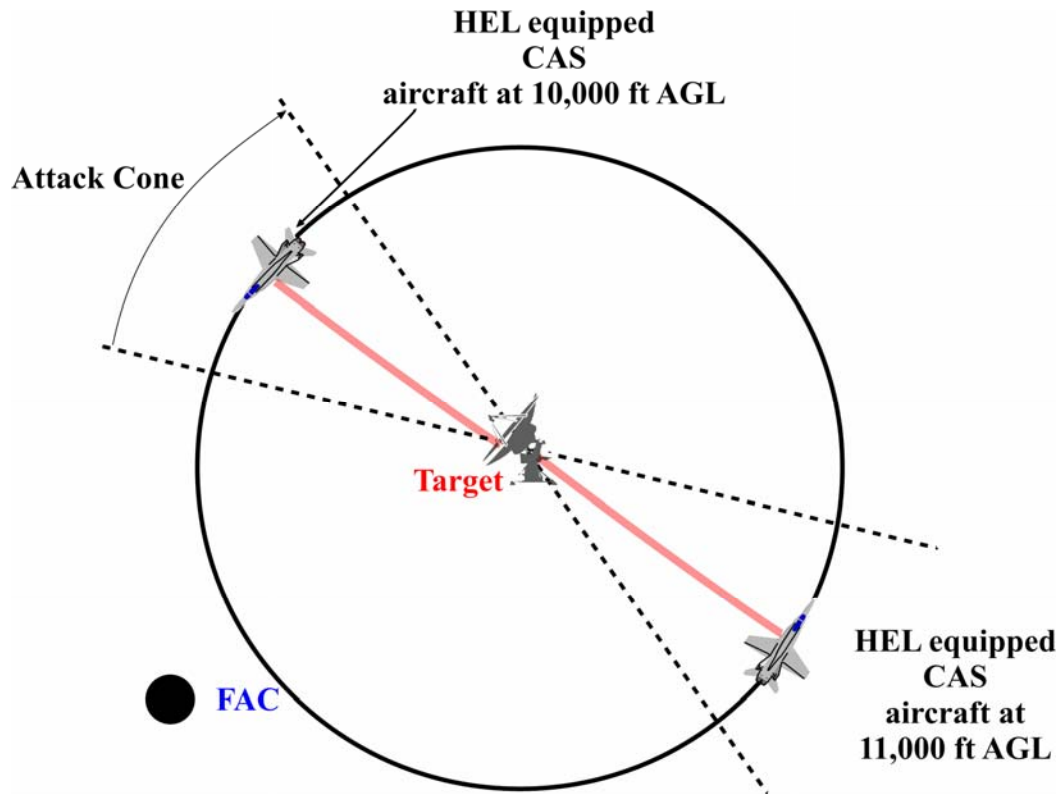


Figure 17. Daytime Low-Threat CAS for HEL-equipped aircraft

In this scenario, the CAS aircraft would be stacked at different altitudes, and in a circular orbit overhead the target. The FAC would talk the aircraft on to the target over the radio, then clear them for the attack (clear them “hot”). A bomb-equipped aircraft would “roll-in” to a dive angle, with its nose pointed at the target, to deliver its ordnance. An HEL aircraft could use the high off-boresight angle capability to track and prosecute the target while remaining at altitude. This could allow the CAS aircraft to acquire and prosecute a new target in a short amount of time. Table 3 lists some of the major advantages and disadvantages of an HEL system in the CAS role.

Table 3. Comparison of HEL and conventionally equipped strike fighter in the low and medium threat CAS role

Variable	HEL	Conventional
On-station time	Limited only by fuel	Limited by fuel and ordnance load
Geometry	No dive required, high off-boresight angle target prosecution possible	Aircraft must be pointed at, or toward the target
Target types	Limited to soft targets only	Hard targets and soft targets, depending on loadout
Weather	Requires good IR visibility, little dust or other aerosols	Can work around weather, ground obscuration not as much of a factor

c. Air Interdiction

Air Interdiction, also called Deep Air Support, is defined as “Air operations conducted to destroy, neutralize, or delay the enemy's military potential before it can be brought to bear effectively against friendly forces at such distance from friendly forces that detailed integration of each air mission with the fire and movement of friendly forces is not required.”³⁹ In tactical naval aviation, interdiction is also referred to as a strike mission.

In this role, an HEL-equipped fighter would be limited by the target type it could effectively prosecute. Hardened targets, such as bunkers, would be poor targets for an HEL system, as the laser energy is not explosive in nature; it burns holes in targets, but does not provide the explosive power necessary to destroy buildings and the like. Targets such as ammunition dumps and fuel farms, however, may be viable options for HEL weapons, if onboard sensors can provide aimpoints that will create secondary explosions (e.g. ignition of high explosive material).

Despite the limited target types, an HEL could still be effective in the strike role, especially with the potential capability to prosecute multiple targets along a strike route. Basic conventional employment on a strike mission is (1) ingress to the target (2) target attack (weapon release), and (3) egress from the target. It is driven both

³⁹ JP 1-02

by the limited weapon loadout and a minimum threat exposure time. An HEL-equipped aircraft, as part of a strike package, could attack multiple soft targets along the ingress / egress route, while conventionally-equipped strikers would attack the hardened targets. Additionally, HEL strikers could also be loaded with air-to-ground weapons, limited by aircraft gross weight for takeoff. Figure 16 below shows a notional concept of employment for an HEL system in the interdiction role.

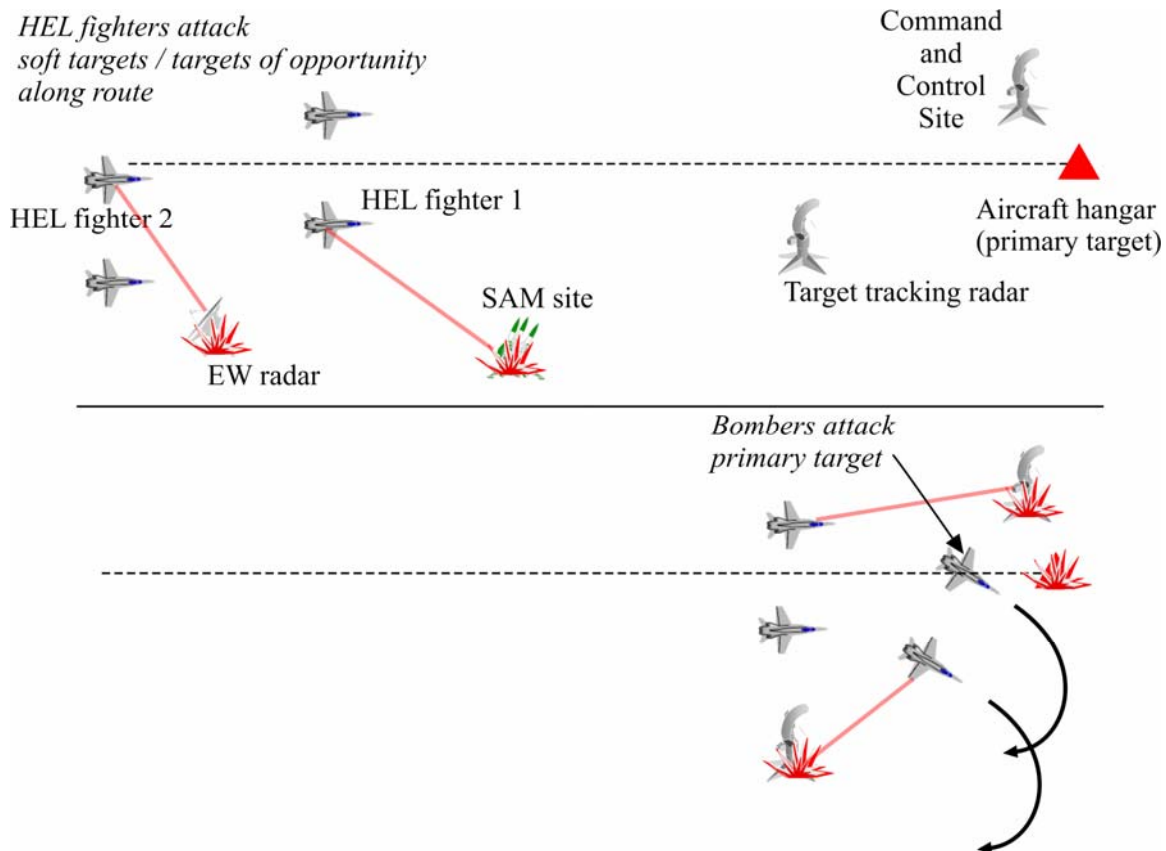


Figure 18. HEL employment for Air Interdiction mission

In the figure above, a strike package of four fighters is ingressing to the target (upper left). Two of the fighters are only equipped with HEL systems, while the others carry conventional loads. As they ingress to the target (top scene), the HEL-equipped fighters prosecute targets of opportunity as well as key air defense nodes. In the target area (bottom scene), the non-HEL fighters prosecute the hardened targets with bombs or other conventional munitions, while the HEL fighters attack softer targets.

Another advantage of an HEL-capable striker is self-escort capability. Typically, strikers will carry a limited air-to-air loadout for self-defense, and thus require some dedicated fighter support. HEL-equipped strike aircraft may have more hardpoints (weapon stations) available for air-to-air weapons, as they would not be necessarily loaded with bombs or other air-to-ground ordnance.

d. Suppression of Enemy Air Defenses (SEAD)

SEAD is defined as “That activity which neutralizes, destroys, or temporarily degrades surface-based enemy air defenses by destructive and/or disruptive means.”⁴⁰ Typically, SEAD for a strike package (such as the one depicted in Figure 16) is provided by active jamming and/or by employment of weapons such as the AGM-88 High-Speed Anti-Radiation Missile (HARM).

The feasibility of an HEL system as a SEAD weapon will be determined by its range capability. As Table 2 shows, the relatively soft components of an air defense radar system may be good targets for laser energy. However, the range of the most widely proliferated long-range surface-to-air missiles (SAMs) greatly exceeds that of most theorized maximum ranges for an HEL weapon. Thus, the HEL fighter would have to enter a SAM threat ring to defeat the weapon, thus exposing itself to the threat. Table 4 shows some maximum ranges of common SAMs⁴¹.

Table 4. Maximum Ranges of Common SAM systems

SAM	Max. Range (nm)	Target Tracking Radar (TTR)	TTR Max. Range (nm)
SA-2D ‘Guideline’	23	FAN SONG C/D/E	40
SA-3B ‘Goa’	10	LOW BLOW	43
SA-6 ‘Gainful’	13.5	STRAIGHT FLUSH	16
SA-8 ‘Gecko’	8	LAND ROLL	11

⁴⁰ JP 1-02

⁴¹ Jane’s Strategic Weapon Systems, Jane’s Information Group, Alexandria, VA, August 2000

As can be seen from the above table, if the maximum effective range of the laser is 5 nm for the SEAD role (high-altitude, air-to-ground), then the attacking aircraft would be well inside the range capabilities for the systems listed.

The role of the HEL fighter in SEAD may be as part of a SEAD package, including a standoff jamming (SOJ) platform and/or as a HARM shooter. With the SOJ platform /HARM shooter (perhaps an EA-6B Prowler or similar aircraft) actively keeping the SAM site from launching, the HEL fighter could safely ingress and engage the TTR or the launcher to effectively destroy the system. In fact, with a highly effective jamming platform, the SEAD package could proceed along a route, perhaps preceding a strike package, eliminating multiple threats along the way.

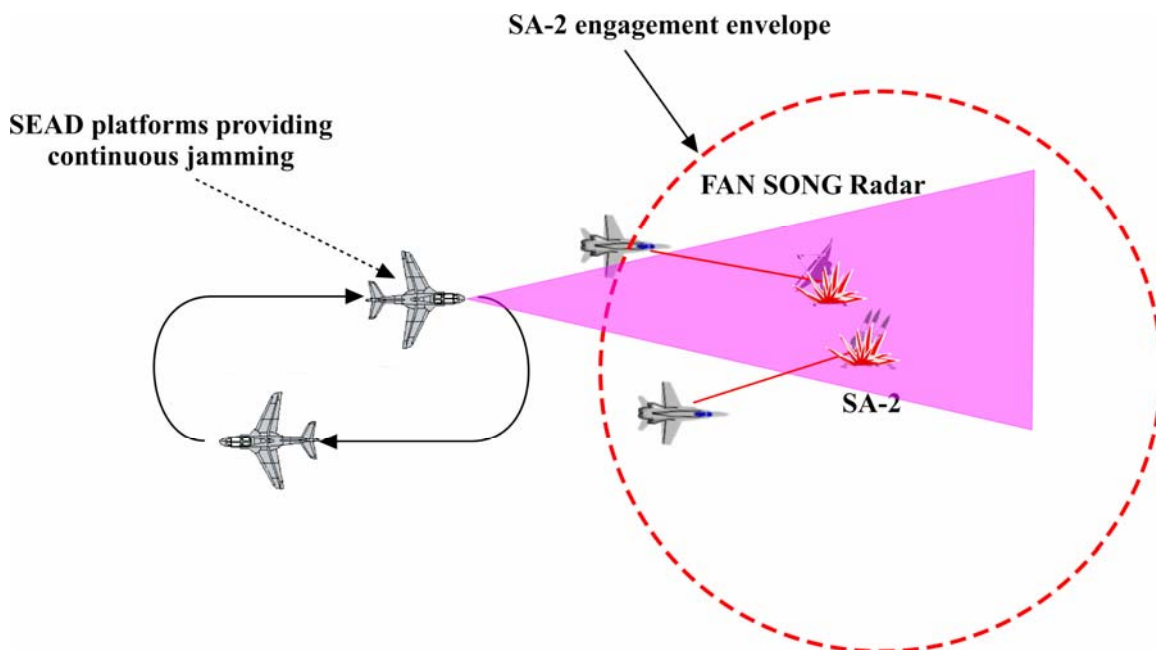


Figure 19. HEL fighter SEAD scenario

Figure 19 depicts a concept of operations for HEL fighters in the SEAD role. Since the laser would not provide adequate standoff for the SA-2 as shown in Table 4, a jamming platform or other means of SEAD would be required for the HEL fighters to prosecute their target (in this case, the launcher and target tracking radar of the SA-2).

e. Surface-to-Air Missile (SAM) Defense

Perhaps the primary threat to any strike platform in the current environment is the SAM. SAMs from the former Soviet Union are widely proliferated throughout the world, and are cheaper and much easier to maintain and operate than an intercept aircraft. SAMs come in two varieties: strategic and tactical⁴². Strategic SAMs, such as the SA-2 and SA-3, are long-range SAMs designed to protect high-value targets (i.e. cities, command and control nodes, etc.). Tactical SAMs, such as the SA-6 and SA-8 are shorter range systems designed to protect mobile battlefield targets, such as troops.

SAM defense is a potential role for an HEL system, and may be the best role for a low-power weapon, but would require a timely and precise cueing/targeting system to keep the laser focused on one spot of the missile. Since the engagement would likely occur at higher altitudes (in the later stages of missile guidance), there would be less atmospheric scattering and absorption, so the power out of the HEL may not need to be as high as with other missions. Also, as discussed earlier, from a lethality perspective, missiles make good targets for laser energy.

Ordinarily, defense against SAMs is a combination of maneuver, chaff deployment, and electronic countermeasures. With an HEL system, maneuvering would be limited by the requirement of maintaining the laser beam on the target without obscuring its field-of-view for somewhere between three to five seconds, nominally. This means that the pilot of an aircraft being targeted by a SAM would need to have a lot of faith in his HEL system, to say the least.

2. Air-to-Air

While the air-to-ground role has been the predominant role of the naval strike fighter in recent conflicts, low altitude employment presents laser propagation problems that high altitude employment does not. Thus, an HEL system might have some significant utility in the air-to-air arena.

⁴² TOPGUN Manual, Naval Strike and Air Warfare Center, August 2003

a. Offensive Counter Air (OCA) / Defensive Counter Air (DCA)

OCA is defined as “an offensive operation to destroy, disrupt, or neutralize enemy aircraft, missiles, launch platforms, and their supporting structures and systems both before and after launch, but as close to their source as possible”⁴³. For the Marine Corps and Navy, OCA is broken down into sweep, escort, and close escort missions. Though the specific tactics of each mission differ, they all result in the attrition of enemy aircraft for the purpose of conducting an offensive operation. In this capacity, an HEL system could function both offensively (i.e. destroying / damaging enemy aircraft) and defensively (destroying incoming air-to-air missiles). As mentioned in the previous subsection, defending against such missiles would require a precise cueing and targeting system, and would be even more difficult than defending against SAMs, which are generally larger and less maneuverable.

DCA is defined as “all defensive measures designed to detect, identify, intercept, and destroy or negate enemy forces attempting to attack or penetrate the friendly air environment”⁴⁴. DCA is divided into point defense, area defense, and high value airborne asset (such as an AWACS or similar aircraft) defense. As with the OCA mission, the HEL could serve in both an offensive and defensive role in the DCA mission.

Figure 18 depicts a notional 2 fighter versus 2 bandit (2v2) HEL OCA or DCA intercept scenario. In (1), two HEL fighters have committed to an intercept against two Mig-29 aircraft with long-range radar-guided AA-10c air-to-air missiles. As the range between the fighters and bandits decreased, the bandits launch missiles (2), which are defeated by the HEL (and a great cueing/tracking system). Then, inside a lethal range (3) for the laser, the HEL is employed against the control surfaces, canopy, intakes, or other vulnerable parts of the bandit aircraft to effect a kill.

⁴³ JP 1-02

⁴⁴ JP 1-02

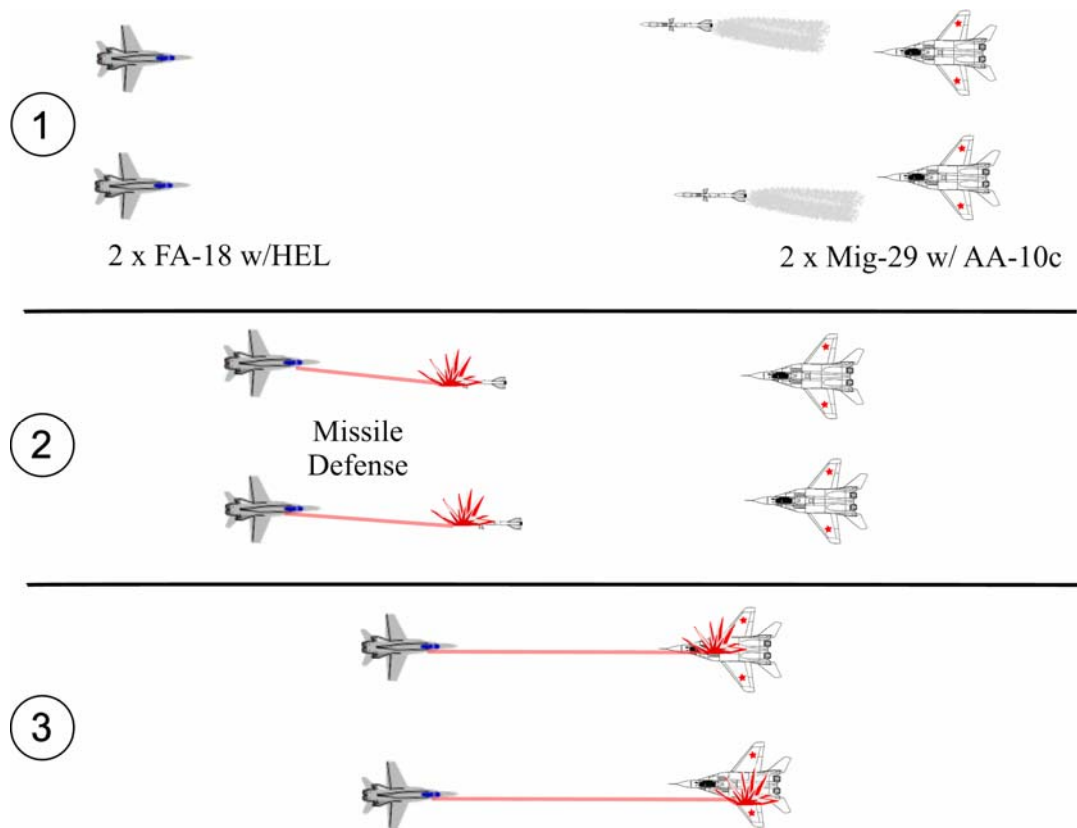


Figure 20. Air Intercept Scenario

b. Air Combat Maneuvering (ACM)

ACM is air-to-air combat within visual range, whereas the above scenarios are conducted beyond visual range. The ACM environment is extremely dynamic and taxing to the aircrew. For both of those reasons, it may not be a feasible mission for the HEL. For one thing, the geometries of ACM engagements are generally such that the aircraft's "lift vector" (roughly the top of the aircraft) is pointed at the enemy fighter. Thus, HEL systems mounted underneath the aircraft would be virtually useless.

Using a "heads out" (i.e. not looking inside the cockpit) cueing system, such as the Joint Helmet Mounted Cueing System, a top- or dual-outcoupled system (as in the potential design of the F-35 HEL system) might have some limited value in the ACM arena. The problem of high G forces, extremely dynamic airflow, and high pilot workload during an ACM engagement still remain.

D. PERFORMANCE CONSIDERATIONS

1. Power Generation

Assuming a 10% wall plug efficiency in a conceptual HEL system (including any cooling and all other subsystems), a 100 kW laser would require an input power of 1 MW. Excess power is not a characteristic of the strike fighter, and so some creative ways of finding and/or generating the required power will be necessary.

a. Joint Strike Fighter

For the F-35 Joint Strike Fighter, the best method of attaining this power may be by coupling the engine on the non-Short Takeoff Vertical Landing variant (F-35B) to one or more high-efficiency generators. The lift fan of the F-35B is capable of producing 82 kN of thrust. This means that over a 9 second vertical elevation to a height of 100m, it is producing ≈ 1 MW of power using maximum vertical thrust.

Assuming that the coupling mechanism to the generator and the efficiency of the generator itself (on the HEL JSF) are equivalent to that of the mechanical coupling of the engine to the lift fan, then the lift fan shaft generator should be able to produce enough power for a 100 kW HEL system.

The generator required for this conversion must be compact, lightweight, efficient, and able to handle the high speed of the turbine shaft. Conventional generators (i.e. non-superconducting) currently used in airborne applications are not able to produce the power levels required for HEL systems. Additionally, the duty cycle for these generators will likely be between one and ten seconds, which is a shorter period of time than current generators. The electrical load of the HEL system will likely be a 200 V rectified DC load ⁴⁵, which differs from most aircraft current systems. The weight of

⁴⁵ Kessler, C. L. "Optimized Conventional Power Generation for High Energy Laser Weapons", Presented at the 2004 Solid State and Diode Laser Technology Review Conference

systems under development is 0.2 lb/kW, and so a 1 MW generator would weigh only 200 lbs.

One key element of such a design is efficiency and thermal management, which are directly related to one another. While the laser will run at a fairly low duty cycle (Time On/[Time On+Time Off] \approx 0.3), a 1 MW generator running with 95% efficiency for 5 seconds will still generate approximately 250 kJ of heat which must be removed prior to the next firing. This is in addition to the heat produced by the laser itself.

Another potential design component is the high temperature superconductor (HTS) generator, which can potentially provide extremely high efficiency, and thus low thermal management requirements. HTS materials, such as $\text{YBa}_2\text{Cu}_3\text{O}_{7-x}$, do not require the extreme low temperatures of standard superconductor materials, and can operate within the temperature range (\approx 70 K) of cryogenic refrigerators⁴⁶. These cryocoolers use compressed helium or other inert gas to provide a cooling medium. This eliminates the need for liquid cryogenic coolant, which is not well-suited to the environment of the tactical strike fighter.

In the classical superconducting generator currently used, the stator is made of superconducting material and cooled. The proposed design for military applications (i.e., JSF) is the all-cryogenic superconducting generator, in which all of the components are made of superconducting materials⁴⁷. In this design, the entire structure could be encased within a cryogenic refrigerator and cooled.

b. FA-18E/F

The FA-18E/F does not have the lift fan that the F-35B has, and its two internal generators are only capable of producing approximately 10 kW of power. Thus,

⁴⁶ Barnes, P., Rhoads, G., Tolliver, J., Sumption, M., Schmaeman, K., "Compact, Lightweight, Superconducting Power Generators", *IEEE Transactions on Magnetics*, Vol. 41, No. 1, January 2005, p. 268

⁴⁷ Barnes, et. al

there will need to be another source of power for the laser. The two most likely candidates seem to be externally-mounted capacitor banks or ram air turbines (RAT) generators, or a combination of the two.

Capacitor banks, housed within an externally mounted pod, are approximately the size of a 450 gallon external fuel tank, with a usable internal volume of approximately 10^6 cm^3 . A three second pulse of laser energy from a 100 kW laser would require: $E = 100\text{kW} \times 3 \text{ s} / 10\% \text{ HEL efficiency} \approx 3 \text{ MJ}$ of energy. Thus, the energy density of one such capacitor bank would need to be approximately 3 J/cm^3 to sustain one engagement. If the capacitor bank could fit within one of the internal avionics bays of the FA-18E/F, it would have to be no larger than approximately 10^5 cm^3 ⁴⁸. The energy density of such a capacitor bank would then need to be 30 J/cm^3 . Capacitors of the former type are under development⁴⁹, while capacitors that fit internally within an avionics bay are not feasible for a 100 kW weapon, or even a 25 kW weapon (a 7.5 J/cm^3 requirement). Thus, the capacitor bank would have to be externally housed.

Rapidly charging such capacitor banks is another issue. The energy stored in a capacitor is given by

$$E = \frac{1}{2} CV^2, \quad (30)$$

where C is the capacitance and V is voltage. The time dependence of the voltage as the capacitor is being charged is given by

$$V = V_f [1 - \exp(-t / RC)], \quad (31)$$

where V_f is the final steady-state voltage, R is the resistance of the circuit, and t is time.

Thus, combining (30) and (31) to obtain the charging time required for energy E :

$$t(E) = -RC \left[\ln \left(1 - \sqrt{\frac{2E}{CV_f^2}} \right) \right] \quad (32)$$

⁴⁸ NATOPS Flight Manual, Navy Model FA-18E/F 165533 and up aircraft, A1-F18EA-NFM-000, Naval Air Technical Data and Engineering Services Command, San Diego, CA, April 2003

⁴⁹ Slenes, K., Bragg, L., "Compact Capacitor Technology for Future Electromagnetic Launch Applications", *IEEE Transactions on Magnetics*, Vol. 41, No. 1, January 2005

It can easily be seen from equation (32) that the greater the charging voltage, the faster the charge time to reach energy E. Unfortunately, the aircraft electrical power available to an HEL on an FA-18E/F with standard avionics is on the order of 10 kW at most, which means that the charging voltage (using a current of 20A for most FA-18E/F electrical equipment) $V = P / I \approx 10 \text{ kW} / 20 \text{ A} \approx 0.5 \text{ kV}$. The designs of future high energy density capacitors (for electromagnetic guns) using dielectric films will require charging voltages of 20-30 kV to charge one capacitor module to 400 kJ in less than five seconds⁵⁰.

One way to create a reasonable charging voltage is the use of a RAT generator. A RAT generator converts mechanical power from airflow over turbine blades into electrical power. RAT generators are used in some naval aircraft as emergency backup systems, as well as augmentation to high power systems (such as the RAT generator on the electronic countermeasures pod of the EA-6B Prowler, which is rated at 30 kW).

Figure 20 shows a concept for a RAT generator within an external pod (note: figure shown is the size of a 300-gallon external fuel tank of an F-16). This design is under development by Ghetzler Aero-Power of Buffalo Grove, IL.

⁵⁰ Wisken, H., Podeyn, F., Weise, T., "High Energy Density Capacitors for ETC gun applications", *IEEE Transactions on Magnetics*, Vol. 37, No. 1, January 2001

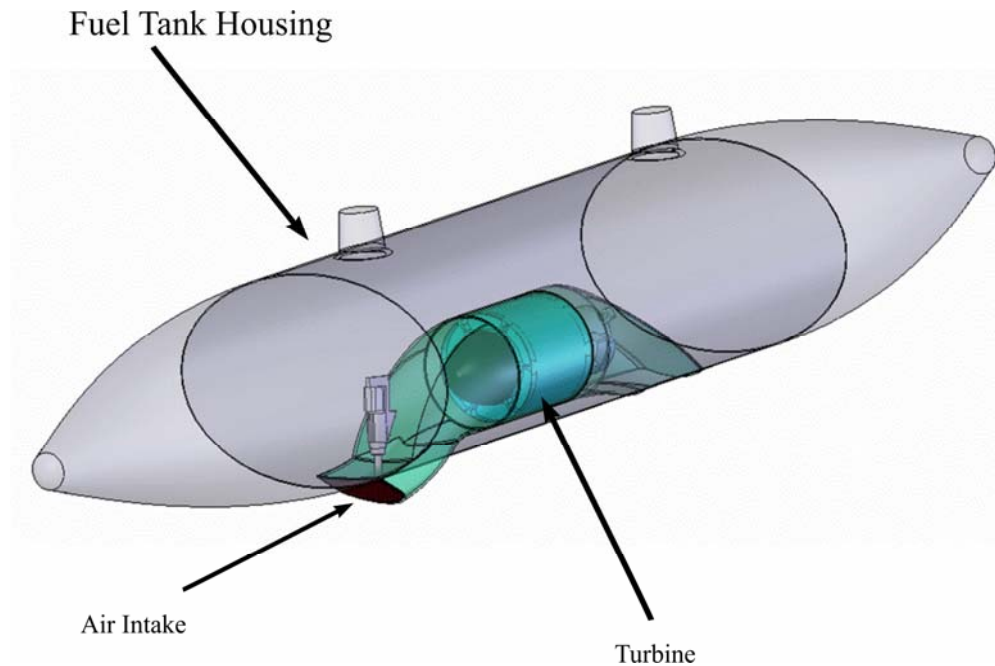


Figure 21. RAT generator concept

2. Thermodynamics

If 1 MW of power is produced and 100 kW of power is outcoupled as laser light, then 900kW remains in the form of heat. This excess heat must be removed quickly for several reasons. As the heat in the lasing medium builds up, the refractive index of the medium is altered by nonuniform distributions of the latent heat. This distortion of the medium alters the mode of the resonator⁵¹, which in turn creates greater losses, as the fundamental (transition) frequency won't survive the effective change in resonator length. The stored heat could also cause thermal fracture, due the differing coefficients of thermal expansion along the rod axis. That is, some sections of the lasing medium will heat and expand more rapidly than others, causing shear and strain forces to damage the medium, and thus render the laser virtually useless.

Another effect of excess stored heat in the medium is optical path distortion at the aperture. The refractive index variations in the lasing medium will create a wavefront

⁵¹ Scheps, R., Introduction to Laser Diode-Pumped Solid State Lasers, SPIE Press, Bellingham, WA, 2002, p.60

distortion, thereby increasing the M^2 value (as in equation (21)) of the beam and degrading its propagation characteristics. A severe distortion of the wavefront will make it very difficult to properly focus the beam on the target with enough intensity to cause damage.

Furthermore, if the heat is not rapidly removed from the aircraft, it could damage or destroy avionics and other subsystems that would be harmed by overheating. Most of these systems (e.g. radar, radar warning receivers, electronic countermeasures equipment) require cooling from an already-taxed engine bleed air system, and a significant amount of heat would be harmful.

Lastly is that any excess heat energy that raises the temperature of some part of the aircraft increases its infrared signature (shifts it closer to the 3 to 5 micron range of most IR detectors) according to Wien's Displacement Law:

$$\lambda_{\max} T = 2.898 \times 10^{-3} \text{ m}\cdot\text{K}, \quad (33)$$

where λ_{\max} is the peak wavelength of the spectral distribution. Thus, for a nominal T of 300 K, the peak wavelength would be approximately 9.7 microns, and a temperature increase to 400 K would bring the spectral peak to 7.2 microns, closer to that 3 to 5 micron band. This is not as critical as the others because it doesn't cause cessation of laser operation.

Any temperature increase alter radiated power, P_{rad} , by the Stefan-Boltzmann Law ⁵²:

$$P_{\text{rad}} = \varepsilon \sigma T^4, \quad (34)$$

where ε is the object's emissivity (ratio of its emissive power to that of an ideal blackbody, always < 1), and $\sigma = 5.6705 \times 10^{-8} \text{ W}/(\text{m}^2\cdot\text{K}^4)$ is the Stefan-Boltzmann constant. Thus, if the temperature of the aircraft component increases from 300 to 400 K, the radiated power increases threefold, mostly in the form of infrared radiation.

Still, the thermal power from the engine exhaust from an FA-18E/F is approximately 40 times that given off by the excess heat of the laser.

⁵² Thornton, S. T., Rex, A., Modern Physics, 2nd ed., Von Hoffman Press, Jefferson City, MO, 2000

a. Thermal Management of the Lasing Medium

For solid-state lasers, heat dissipation will be a two-step process. First, the heat must be removed from the lasing medium. For conventional lasing media (i.e. non-fiber), this is a challenge. For a crystal medium, the surface area from which heat can escape compared to the lasing volume is insufficient to support adequate cooling for high-energy applications. One technique, under development at Lawrence Livermore National Laboratory, is the solid-state heat capacity laser, which is an array of diode-pumped neodymium-doped gadolinium gallium garnet (Nd:GGG) slabs. Essentially, this 10 kW laser operates until the lasing medium temperature reaches a certain critical level. Then, the lasing is brought to a halt and the cooling cycle starts. Cooling is achieved by coolant water pumped to each of the slabs between cycles. In this fashion, the laser is able to operate for up to ten seconds out of every minute⁵³. The disadvantage is the requirement for a liquid cooling system, although it still could be feasible on the JSF. For the FA-18E/F, a pod-mounted laser with its own internal liquid cooling system would be required.

Another option for consideration is the fiber laser, discussed previously. The fiber laser medium has a much larger surface-to-volume ratio than traditional solid-state lasers. Essentially, the heat has less distance to travel to escape. Additionally, it has been demonstrated that using a distributed pumping scheme instead of an end-pumped scheme (such as those shown in Figs 9 and 10 in section I.C) can cause the generated heat to be distributed and dissipated uniformly⁵⁴. This may make it possible to achieve powers in the kilowatt class, with adequate heat dissipation from the medium. Photonic crystal fiber lasers, as discussed earlier, could potentially serve one or two purposes. One of the drawbacks of using long (> 1 m) fibers is the likelihood of nonlinear effects such as stimulated Raman scattering causing transverse mode degradation. The solution may be shorter, rod-like large mode area photonic crystal fibers, which retain the advantages

⁵³ H. Jones-Bey, H., "Livermore Targets Battlefield Environment", *Laser Focus World*, December 2003

⁵⁴ Wang, Y., "Heat Dissipation in Kilowatt Fiber Power Amplifiers", *IEEE Journal of Quantum Electronics*, Vol. 40, No. 6, June 2004

of the fiber laser while eliminating the nonlinear effects⁵⁵. The tiny holes in these lasers increase the surface area and allow heat to escape more rapidly than with a typical large mode area fiber laser. Additionally, high-pressure fluid, such as aircraft engine bleed air, could be pumped through the holes to carry the heat away from the laser and surrounding systems.

b. Thermal Management of Surrounding Airframe Components

Once the heat has been removed from the lasing medium, the more challenging process is to remove it from the aircraft itself. One possibility is to use fuel flow to carry the heat to the wing fuel tanks, where it is conducted into the wing and dissipated into the airstream by convection. This technique is used to dissipate heat from avionics systems and excess engine heat, and could be used for an HEL system as well. Figure 22 is a conceptual picture showing how this might work on an FA-18E/F, although similar numbers would apply to the JSF as well.

Note that the numbers shown in figure 22 are estimates, and are based on calculations using an outside air temperature of -20°C , and airspeed of 400 knots. Air density variation was not accounted for, and the areas of conducting airframe surfaces were approximated. Also, the heat generated by the aircraft avionics and excess engine heat are not shown.

Still, it appears that there is plenty of cooling ability using this method. The real problem lies with the heat transport to and through the fuel system. For the FA-18E/F, with an externally-mounted pod, fuel would need to be routed through the pod and over a heat exchanger with the HEL system. The flow rate of the cooling fuel will be limited by the existing fuel plumbing for the external fuel tank, which may pose a problem.

⁵⁵ Limpert, J., Deguil-Robin, N., Manek-Honninger, I., Salin, F., Roser, F., Liem, A., Schreiber, T., Nolte, S., Zellmaier, H., Tunnermann, A., Broeng, J., A. Petersson, A., Jakobsen, C., "High-power rod-type photonic crystal fiber laser", *Optics Express*, Vol. 13, No. 4, 21 February 2005

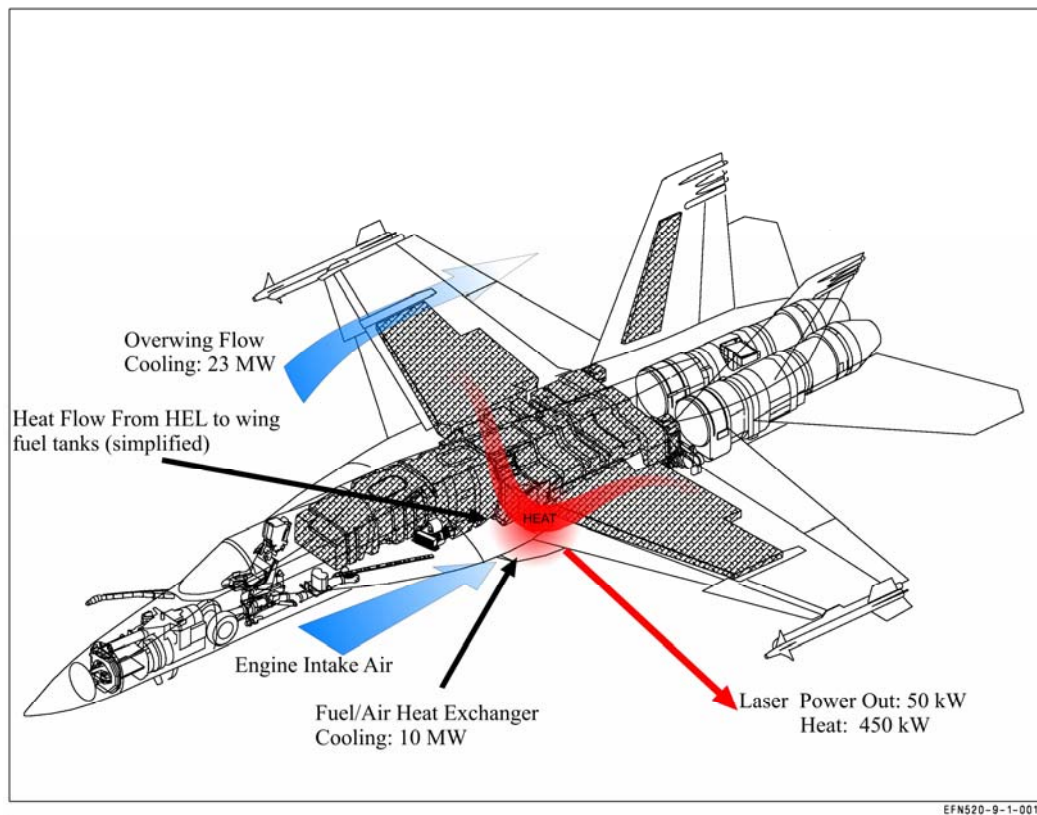


Figure 22. Notional Heat Flow Concept for FA-18E/F

For the JSF, the internal configuration of an HEL system may allow larger fuel lines and multiple heat exchangers to carry the heat away from the HEL system. This may make the heat transport in the JSF more feasible than in the FA-18E/F.

3. Aero-Optic Effects

The propagation of the laser beam after it leaves the aircraft is degraded by many factors. The airflow around the aircraft can be a turbulent boundary layer that can act as a lens right at the source of the beam, either spreading the beam or shifting its aimpoint (called beam “wander”). Likewise, the turbulence inherent in the atmosphere can vary greatly, and can cause beam spreading anywhere along the beam path. It can also distort the wavefront so that the intensity profile at the target becomes distorted. Atmospheric absorption and scattering, at the molecular and aerosol levels, will attenuate the beam power. Thermal blooming, which is essentially superheated stagnant air around the laser

beam causing lensatic effects, is not a factor of concern when dealing with fast-moving aircraft, because the crossing rate of the beam is sufficiently fast to prevent any latent heat from gathering in the air surrounding the beam.

a. Turbulence

By combining Equations (21) and (24), it can be seen that the effect of the beam quality, characterized by M^2 , on diffraction is

$$w(Z) = M^2 \left(\frac{\lambda Z}{\pi w_a} \right) \quad \text{for } Z \geq z_0, \quad (35)$$

where Z is the propagation distance (range), λ is the wavelength, and w_a is the beam director aperture radius. The strength of turbulence is quantified by a value of C_n^2 , which is called the structural value of the index field, or the index structure constant. Values for C_n^2 have been determined for different scenarios by experimentation⁵⁶. The commonly-used values for weak, moderate, and strong turbulence are as shown in Table 6.

Table 5. C_n^2 Values for Different Turbulence Models

Turbulence Level	C_n^2 (m^{-2/3})
Weak	10^{-17}
Moderate	10^{-14}
Strong	10^{-13}

Adding the effects of turbulence to equation (35) gives

⁵⁶ Zuev, V. E., Laser Beams in the Atmosphere, Plenum Publishing, New York, NY, 1982, p. 192

$$w(Z) = M^2 \left(\frac{\lambda Z}{\pi w_a} \right) + 2 \left(C_n^2 / \lambda^{1/3} \right)^{3/5} Z^{8/5} \quad (36)$$

which gives the beam radius at the target including the effects of turbulence. As an example, if $M^2 = 2$, $\lambda = 1.06 \mu\text{m}$, $w_a = 0.1 \text{ m}$, $z = 5 \text{ km}$, $C_n^2 = 10^{-14}$ (moderate turbulence), then $w(Z) \approx 13 \text{ cm}$ as opposed to approximately 3 cm with no turbulence effects included. Additionally, beam wander effects are given by⁵⁷

$$\rho_{\text{wander}} \cong 1.14 \left(\frac{z}{w_0} \right) \left(\frac{C_n^2 z}{w_0^{1/3}} \right)^{1/2} w_0 \quad (37)$$

where ρ_{wander} is the shift of the beam centroid from the aimpoint. Thus, for the same parameters as the above example, the beam centroid shift ρ_{wander} would be approximately 6 cm , which is significant for a laser weapon dependent on concentration of energy in a very small area.

The beam distortion effects due to turbulence can be modeled using random phase screens. A random phase screen at one or more points along the propagation of a laser beam within a simulation assigns a randomized shift in phase to different positions the transverse wave front. This has the same effect as atmospheric turbulence, which creates tiny pockets of differing densities and thus refractive indices. The effect of a random phase screen on the wavefront can be given by

$$\xi_{\text{out}}(x, y) = e^{-i\phi_r(x, y)} \xi_{\text{in}}(x, y) \quad (38)$$

where ξ_{in} and ξ_{out} are the complex electric fields of the beam at that particular coordinate going into and coming out of the phase screen, respectively. The quantity ϕ_r is a random phase angle. Phase screen operators are applied at one or more points along the propagation path to simulate turbulence.

Figure 23 shows the final cross-sectional intensity plots (at the target) of an initially perfect Gaussian beam exiting an infinitely large aperture, with and without turbulence. Note the distortion of the intensity profile due to the turbulence effects. This

⁵⁷ "Laser Beam Propagation in the Atmosphere", brief by Dr. Philip Sprangle at the 2004 Directed Energy Symposium, Rockville, MD

simulation was performed using a series of twenty random phase screens to simulate turbulence along the entire propagation path.

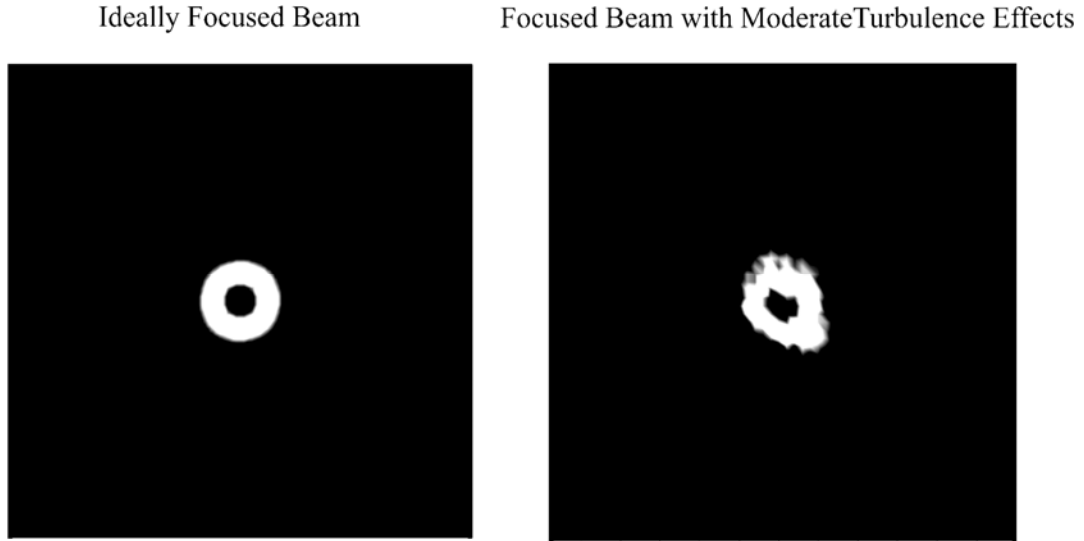


Figure 23. Turbulence Effects on Transverse Intensity

To more accurately illustrate the spreading effects of turbulence, simulations were performed using the High Energy Laser End-to-End Operational Simulation (HELEEOS). HELEEOS is a code developed at the Air Force Institute of Technology Center for Directed Energy, and can be used to simulate engagement scenarios using notional HEL systems, different atmospheric conditions, and different altitudes and airspeeds. Figure 24 shows the results of a simulation using HELEEOS with the following parameters: $z=3$ km, Altitude (shooter and target) = 3000 feet, closing velocity (between Shooter and Target) = 600 m/s , and $C_n^2=10^{-14} \text{ m}^{-2/3}$ (moderate turbulence) and 0 (for comparison).

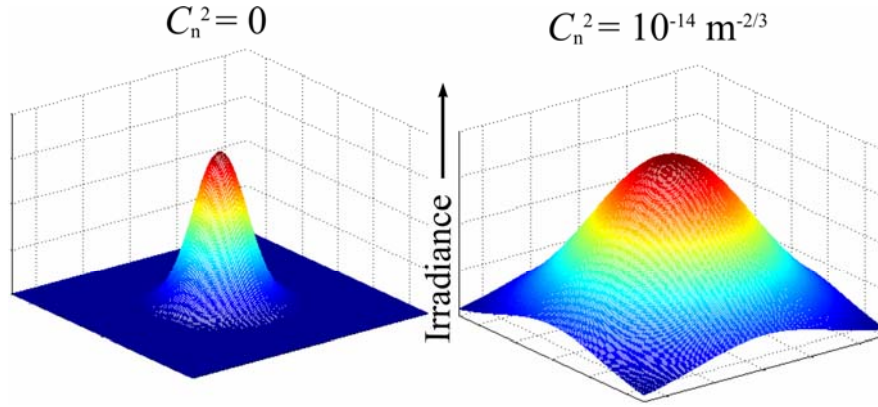


Figure 24. Beam Spreading Effect of Moderate Turbulence for Co-Altitude Shot

Note that in Figure 25, there is no attenuation, as absorption and scattering effects were neglected. However, it is clear the irradiance profile of the turbulent scenario is much wider than the non-turbulent one, and thus the energy on target is much less concentrated. Also, there are no random phase screens used in this calculation, only beam spreading based on Equation (36).

To compensate for the effects of turbulence on beam propagation, an adaptive optics system, using deformable mirrors or similar technology to correct wavefront aberrations, will need to be utilized.

b. Absorption and Scattering

Extinction of the laser beam energy by the atmosphere is due to the effects of absorption and scattering. Atmospheric absorption is of two types: (1) molecular absorption, and (2) aerosol absorption. Molecular absorption is the absorption of photons at the molecular level, similar to the excitation process described previously for stimulated emission. Aerosol absorption occurs when particulates such as dust and water droplets absorb photons.

The three atmospheric scattering processes which can affect electromagnetic radiation propagating through the atmosphere are Mie, Rayleigh, and Raman scattering. Mie scattering, for wavelengths on the order of or less than the

particle size, is the type that affects infrared laser light. Like absorption, scattering occurs at both the molecular and aerosol levels, with the aerosol scattering being the dominant process⁵⁸.

The intensity (power per unit area) $I(Z)$ of light reaching the target at range Z is given by

$$I(Z) = I_0 \exp(-\chi Z), \quad (39)$$

where I_0 is the initial laser intensity at the source, and χ is an extinction coefficient that includes both absorption and scattering. Extinction χ is defined as

$$\chi = \alpha + \delta \quad (40)$$

where α is the absorption coefficient and δ is the scattering coefficient. Furthermore, α and δ can be further defined by their molecular and aerosol components, such that $\alpha = \alpha_a + \alpha_m$ and $\delta = \delta_a + \delta_m$. As an example, starting with a 100 kW laser, it would provide 100kW/cm² intensity on a spot of 1 cm² area if extinction $\chi = 0$. However, if the extinction coefficient is $\chi = 0.3 \text{ km}^{-1}$ (an approximate low-altitude rural environment value) at a range of 5 km, then the intensity on target would be only 22 kW/cm². From Table 2 it can be seen that this intensity wouldn't be effective against light armor, but might be effective against a radar dish or SAM nosecone.

The extinction coefficients are very wavelength-dependent, and in fact are the primary factor when selecting a wavelength for weaponized HELs. There are atmospheric transmission “windows”, or wavelength bands, where the extinction coefficients are sufficiently low to allow adequate propagation. Figure 26 shows the atmospheric transmission windows at sea-level, which shows the percentage of the original intensity at the target after an 1800 meter horizontal propagation.

⁵⁸ Sprangle brief

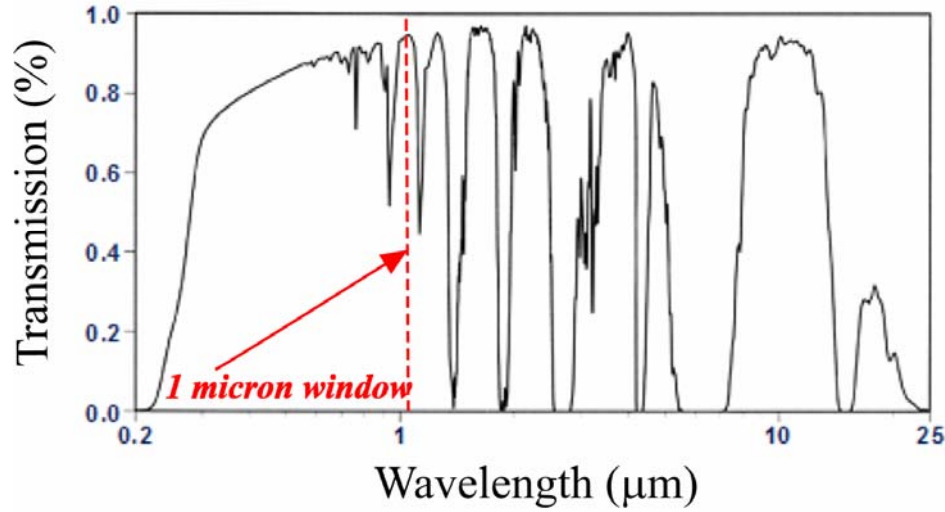


Figure 25. Atmospheric Transmission Windows at Sea Level

It can be seen that the 1 micron wavelength is within one of the transmission windows, and thus most military laser applications to date are in that range. Note that there are also adequate transmission windows at 3 to 5 microns, as well as a large window at 10 microns. These wavelengths may too be feasible, although diffraction effects as per equation (35) make them a less attractive option.

Extinction is also a factor of altitude, and there will be a different transmission curve such as the one shown in Figure 26, for each altitude. HELEEOS uses molecular and aerosol models (standard or user defined) to provide an estimate of extinction at different altitudes, and from one altitude to another. For example, using the HELEEOS rural aerosol model of 15000 parts per cm^2 and the “U.S. 1976 Standard Atmosphere” model for molecular composition at an altitude of 3000 feet, the values of the extinction coefficients are $\alpha_a = 0.007 \text{ km}^{-1}$, $\alpha_m = 0.009 \text{ km}^{-1}$, $\delta_m \approx 0$, and $\delta_a = 0.05 \text{ km}^{-1}$. Thus, aerosol scattering is the dominant process, and the total extinction coefficient is $\chi = 0.066 \text{ km}^{-1}$.

To determine the potential effectiveness of three different laser power levels in both the air-to-air and air-to-ground scenarios, HELEEOS simulations were performed using rural aerosols (as above), “Hufnagel Valley 5/7” turbulence model, and standard atmosphere (as above), from four different altitudes (different for each

scenario). All scenarios include a 5000m ground range from the target to the aircraft, for simulated standoff capability, and slant ranges are calculated from there. Figure 27 shows the approximate power on a spot size at the target of approximately 75 cm^2 for the air-to-ground scenario for a 25 kW, 50 kW, and 100 kW HEL weapon. A simulated solid-state system with beam quality $M^2 = 1.3$ was used.

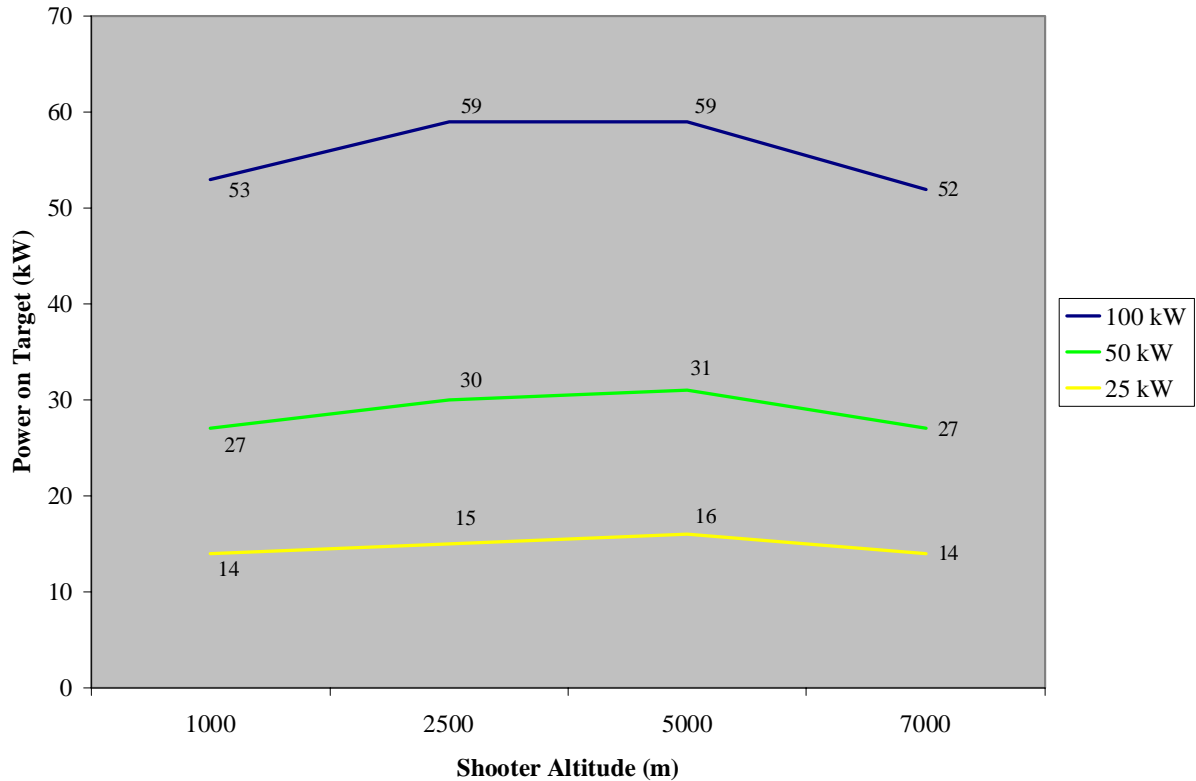


Figure 26. Plot of Power on Target vs. Altitude for Air-to-Ground Scenario

From Figure 26 it can be seen that for an air-to-ground scenario, (1) a 25 kW laser will be very limited at any altitude as to target type, and (2) the mid-altitudes of 2500 m and 5000 m seem to be the best employment altitudes if the threat environment allows.

Figure 27 shows a plot of the approximate power on target for the air-to-air scenario. The target is at a range of 5 km and co-altitude with the shooter in this case. Again a spot size at the target of approximately 75 cm^2 and a beam quality of $M^2 = 1.3$ was used.

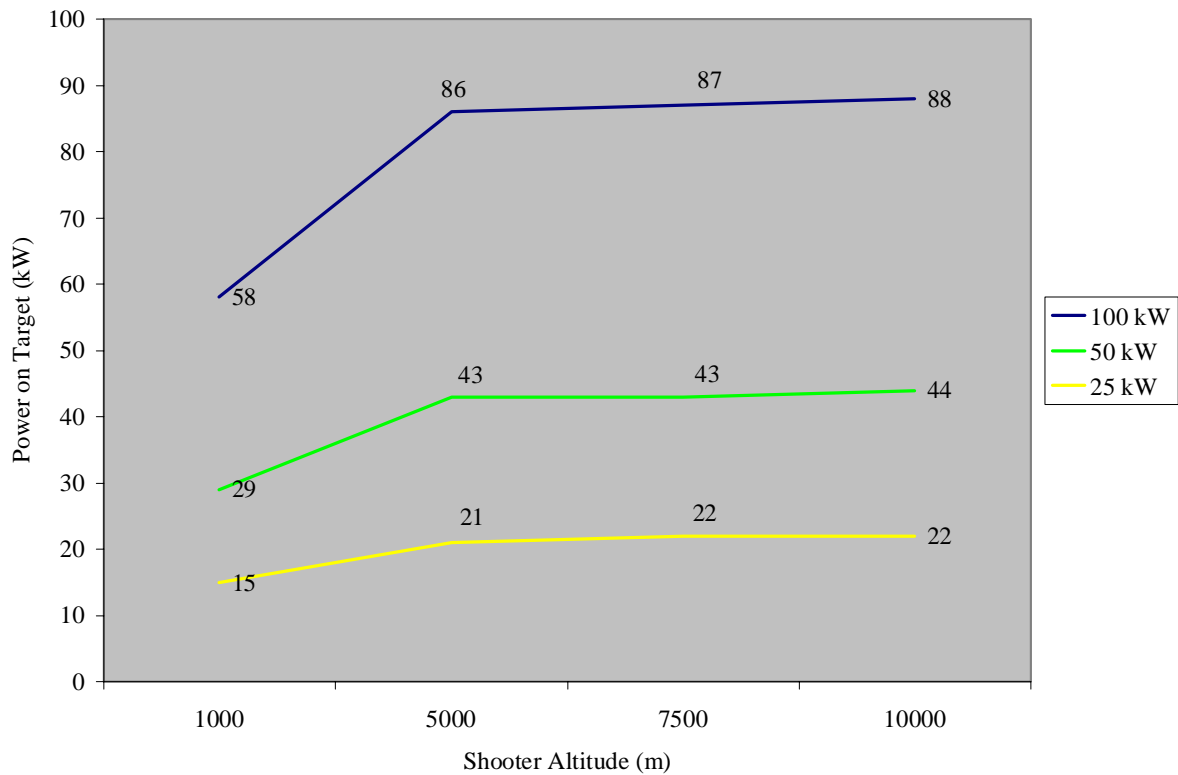


Figure 27. Plot of Power on Target vs. Altitude for Air-to-Air Scenario

From Figure 27, it is clear that (1) the 25 kW laser may have some utility in the mid-to-high altitude air-to-air regime, and (2) above 5000 m, the beams become diffraction limited, and thus there don't seem to be significant advantages to higher altitudes. This is counter to typical air-to-air engagements, where a high altitude increases missile ranges dramatically, and thus higher is better.

The last simulations performed with HELEEOS were to determine the power on target in an air-to-air engagement at an altitude of 10000 m (approximately 30,000 ft) at various ranges. The same general beam quality, target, and atmospheric parameters listed above were used. The results of these simulations are shown in Figure 28, and show that a 100 kW, and even a 50 kW laser in an air-to-air scenario, could be used at effective employment ranges.

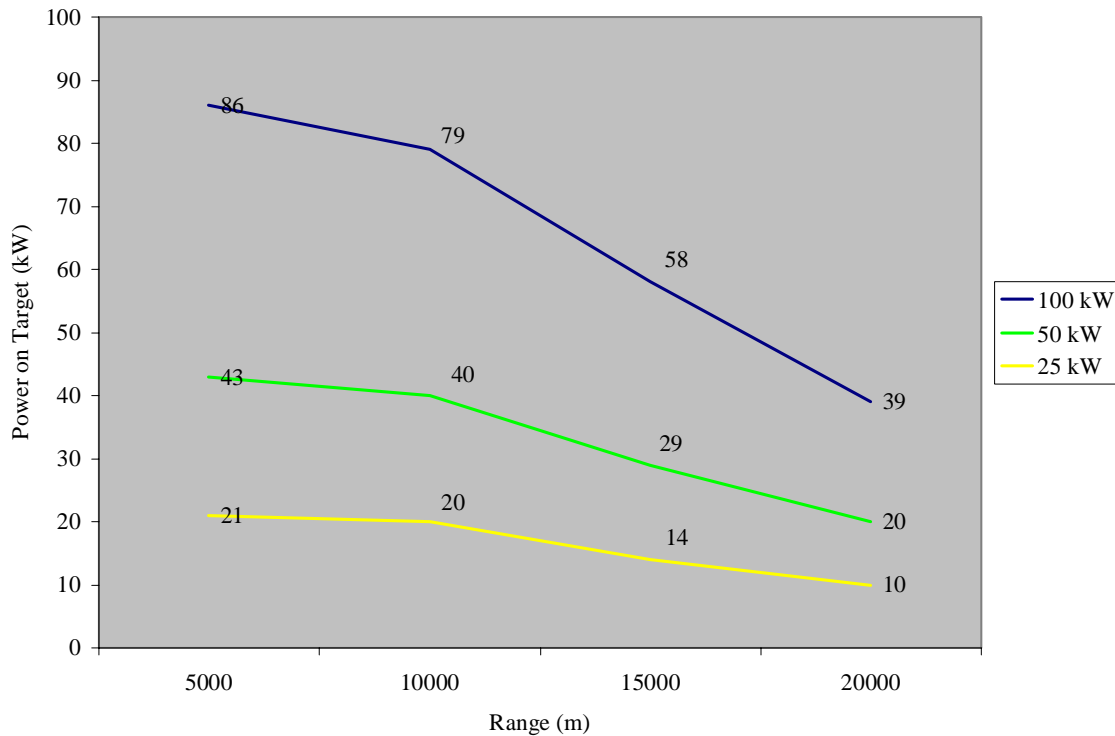


Figure 28. Plot of Power on Target vs. Range for Air-to-Air Scenario

E. CONCLUSIONS

It has been shown that there are many physical considerations in the employment of high energy solid-state laser systems aboard fighter-sized aircraft. However, with developing technology, none are insurmountable. The real question is whether or not such a system is worth the time and money spent to research, test and field these new technologies.

For the FA-18E/F, the likelihood of being able to field a thermally-managed, adequately-powered 100 kW laser system is low. And, while a 50 kW system appears (via HELEEOS simulation) to be an adequate air-to-air offensive and/or defensive weapon, its utility in the air-to-ground environment would be somewhat limited to the softer targets. Clearly, a 25 kW system will be inadequate in the air-to-ground environment. However, it could prove to be a decent defensive air-to-air weapon (in the

SAM defense role). Diffraction effects make the power on target at ranges greater than 10 km too small to be effective, and thus it would have little tactical value in the offensive air-to-air role. The versatility of an HEL weapon makes it an attractive option for the warfighter. If a 50 kW or greater weapon could be fielded on an FA-18E/F, then it could prove to be a valuable asset. A 25 kW weapon, serving only as a defensive, close-range system, might be too much of a sacrifice of weapon stations and fuel carrying capacity for the Super Hornet.

The Joint Strike Fighter should be able to adequately power a 100 kW weapon. The question of cooling remains, although those technologies are under development. A 100 kW system is clearly versatile in both the air-to-air and air-to-ground environments, and this weapon would revolutionize the tactics of the aerial arena. Again, though, it will never be a standalone weapon. There will always be a need for explosive weapons and hard target penetrators to destroy certain targets. There will always be scenarios where the laser, no matter how powerful, will be relatively useless (e.g. bad weather), and thus there will always be a need for the conventional weaponry of the strike fighter.

THIS PAGE INTENTIONALLY LEFT BLANK

III. THE FREE ELECTRON LASER AS A TACTICAL AIRBORNE WEAPON

A. CONCEPT EVOLUTION

The concept of the free electron laser stemmed from earlier uses of electron beams to produce electromagnetic radiation. In the 1930s, the microwave tube was developed, which used a beam of non-relativistic electrons inside a closed cavity to produce microwaves. The earliest of these tubes was the inductive output tube (IOT), wherein an electron beam travels between electrodes inside a closed toroidal cavity, and power is extracted from the beam in the form of electromagnetic radiation without intercepting the beam itself. The IOT was soon followed by the klystron, which simply added an input resonator to the cavity so that the beam was composed of electrons traveling at different velocities that later bunched. The klystron is still used in many applications today.

The combination of the above idea with the knowledge of lasers already established led to the development of the FEL. In 1971, the concept of using relativistic electrons to produce laser radiation was born. Using a beam of free electrons similar to that used in the klystron (though at much higher energy), and an optical resonator as is used in the molecular lasers, light energy was extracted from electrons by passing them through an undulating magnetic field.

B. FEL COMPONENTS

The primary components of the FEL system are the photoinjector, electron accelerator, undulator, and resonator. Below is an illustration of the basic system arrangement.

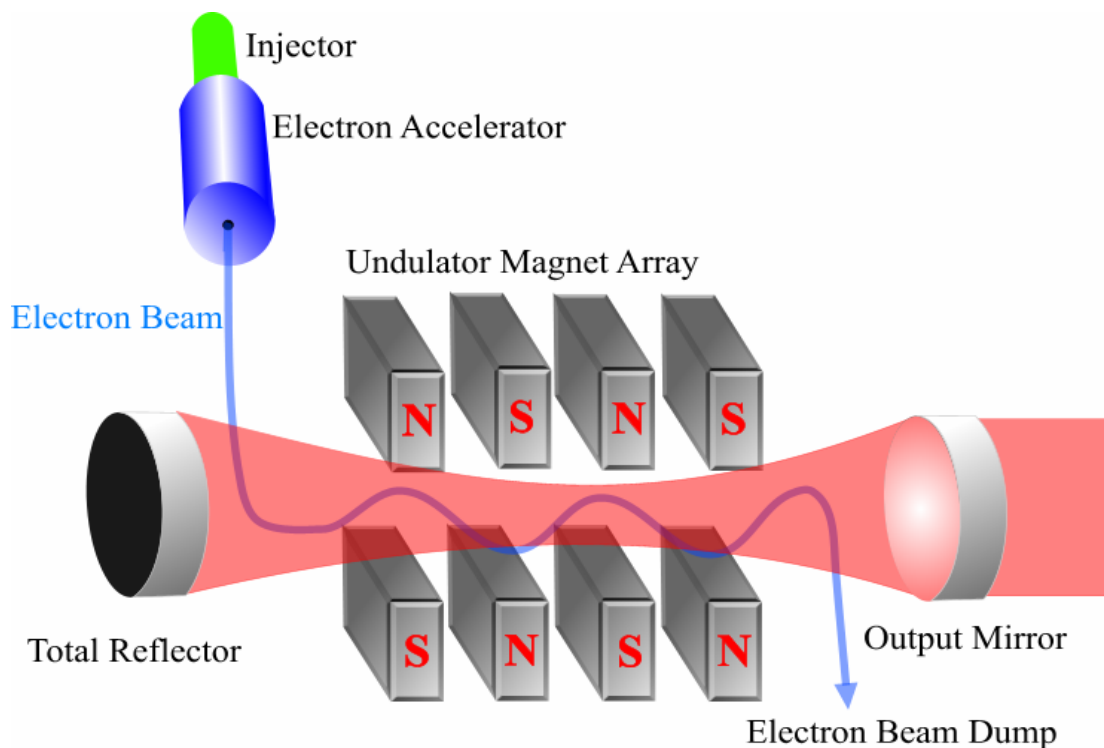


Figure 29. Basic Components of an FEL System

The photoinjector (not shown in Figure 20) consists of a laser and a photocathode. Pulses of laser energy cause the photocathode to eject the electrons in groups, referred to as “micropulses”. A typical pulse length is on the order of 1 picosecond, with an energy on the order of 10s of MeV. The pulse repetition frequency (PRF) of the drive laser (typically around 700 MHz) is such that the spacing between bunches is optimized, which allows greater average power output. The electrons then go into the electron accelerator, but the PRF of the drive laser must be a multiple of the accelerator RF frequency so that each micropulse is accelerated.

In the electron accelerator, RF energy is used to further accelerate the electrons to higher relativistic energies. After the electrons are accelerated, they are injected into the resonator cavity just prior to the undulator. The undulator, or “wiggler” consists of a series of periodically alternating linear magnets (a linear undulator), or wires wrapped around the cavity in a spiral to produce a magnetic field that rotates as the electrons travel down the undulator (a helical undulator). A typical wiggler period is a few centimeters, although these can vary somewhat. Both types of undulators have the same general

effect; Lorentz forces act on the moving charges inside the magnetic field to cause accelerations. Radiation in the form of light is emitted along the electron. After the electrons have traveled the length of the undulator, they are sent to an electron dump or recycled through the accelerator to recover energy.

The resonator is an optical cavity bounded by a highly reflecting mirror on one end and a partially reflecting mirror on the other. The undulator is also contained within the resonator. Similar to other types of lasers, the photons emitted from the electron acceleration in the undulator are bounced back and forth inside the resonator, taking energy from the undulating electrons up to a saturation point. The light is continually transmitted through the partially reflecting mirror as the output laser beam.

C. PROPERTIES OF FEL SYSTEMS

There are several advantages that the FEL has over solid-state and other laser systems. First, the wavelength of the laser is continuously tunable, meaning that the laser can be modulated over a certain bandwidth if another wavelength is desired. The wavelength of the optical laser beam is directly related to the energy of the electron beam and the properties of the undulator, which can be adjusted within some range.

FELs can be designed to emit microwave, infrared (the most common for weapon applications), visible, ultraviolet (UV), or X-ray radiation. The output wavelength of the beam, in addition to the dependence on the electron beam energy, is also dependent on the magnetic field strength of the undulator. This field strength, as well as the undulator period can be set as necessary to produce the desired wavelength.

The lasing medium contains only the undulator field, laser light, and the electron beam in a vacuum (actually very nearly a vacuum), which, unlike its molecular and chemical laser counterparts, does not retain heat created during the lasing process. Instead, any heat generated by the accelerating electrons is carried away by those same electrons at nearly the speed of light. Thus, the cooling requirements for the lasing medium are less, and the laser is not power-limited by its heat capacity.

In order to make the system more efficient, the spent electron beam can be recycled to recover energy. This allows the FEL to anticipate a wall plug efficiency of approximately 10%.

D. FREE ELECTRON LASER INTEGRATION INTO TACTICAL AIRBORNE PLATFORMS

The size and weight of a Free Electron Laser system tends to be thought of as an insurmountable issue for integration into an airborne platform. What follows is a brief discussion of a physics-based design for an FEL aboard a C-130J-30 Super Hercules aircraft. The AC-130 Spectre aircraft, in the field for many years, has proven the utility of a long time-on-station gunship, although its target set is somewhat different. Included are some possible methods to reduce the size, weight, and energy requirements of the system. Reductions of these parameters from those in existing FEL designs would be prerequisite to implementing this system onto a C-130J-30, or any other aircraft.

1. C-130J-30 Constraints

The volume of this FEL design is actually comparable to that of some shipboard systems. The size and weight specifications of the C-130J-30 are shown in Figure 30.

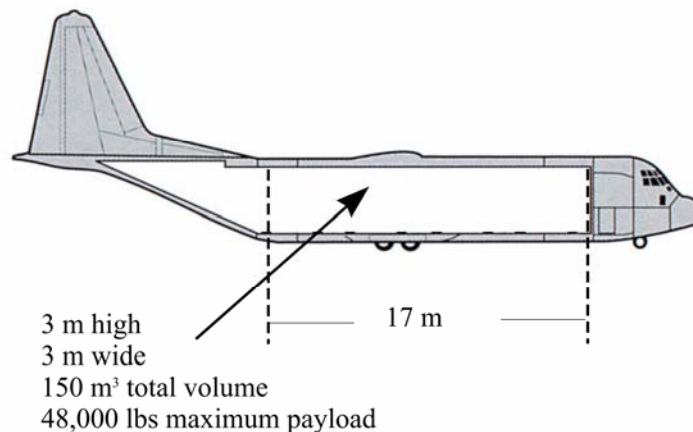


Figure 30. C-130J-30 General Specifications

Some shipboard FEL designs have total system weights of approximately 120,000 lb, and so it can easily be seen that the weight of the airborne FEL system presented will be a major limiting factor.

The C-130J-30 is a 4 engine aircraft, with each engine attached to a 40 kW generator. To power a 350 kW laser operating at 10% wall plug efficiency, 3.5 MW of power is needed. Clearly an independent power source will be required. Studies are underway to examine the feasibility of high-power generators, mechanical flywheel generators, and power-conditioned capacitors to power this system.

2. Integration Considerations

The wavelength of the FEL is selected based on minimization of collateral damage, which is something that must be considered for any weapon. One possible way to do this is to choose the fixed optical wavelength of $\lambda = 1.625$ microns. The main advantage of this is that 1.625 microns is a relatively “eye safe” wavelength. That is, that particular wavelength does not damage the retina of the human eyeball at low intensities. This would make the weapon more suitable to precision missions with friendlies and/or non-combatants in the vicinity of the target.

There are some possible methods to reduce the weight and increase wall plug efficiency of a typical FEL design, although some sacrifices in performance must be made. By using a fixed wavelength, permanent magnets could be used to supply the main magnetic fields for electron beam steering. These would be augmented by trim coils for fine tuning of the field, but would potentially decrease the weight and increase the wall plug efficiency.

The refrigerated liquid helium (LHe) system cooling the accelerator could instead be replaced by a 4K LHe cryostat. This cryostat would simply be a tank of LHe that would boil off to dissipate heat generated by the accelerator cavity. In order to do this, studies need to be performed to determine the feasibility of a 4K-cooled RF cavity that

can produce an accelerator gradient of approximately 10 MeV/m. This system would reduce the gross weight by not requiring pumps and other heavy refrigerator equipment. Additionally, it could increase the wall plug efficiency, since little power would be needed to operate it. The helium is expendable, of course, and would be replaced as often as lasing time dictated.

Electron beam energy recovery will also be used as part of a weight and power reduction effort. This reduces the need for RF power, shielding in the aircraft, and amount of heat removal required in the beam dump.

3. 350 kW FEL Parameters

Table 6 lists the parameters used for a simulation (described in Sec. IV.D.4) of the 350 kW airborne FEL. Figure 31 below shows a diagram of a design concept for FEL integration into a C-130J-30.

Table 6. 350 kW FEL Simulation Parameters

Peak Current	250 A	Beam Energy	80 MeV
Avg Current	0.15 A	Bunch charge	0.2 nC
Magnet gap	1 cm	Micropulse frequency	750 MHz
Peak B	0.8 T	Optical outcoupling	25%
Mirror Spacing	16 m	Pulse length	0.8 ps
Number of Periods	20	Emittance	5 mm-mrad
Undulator spacing	2.7 cm		

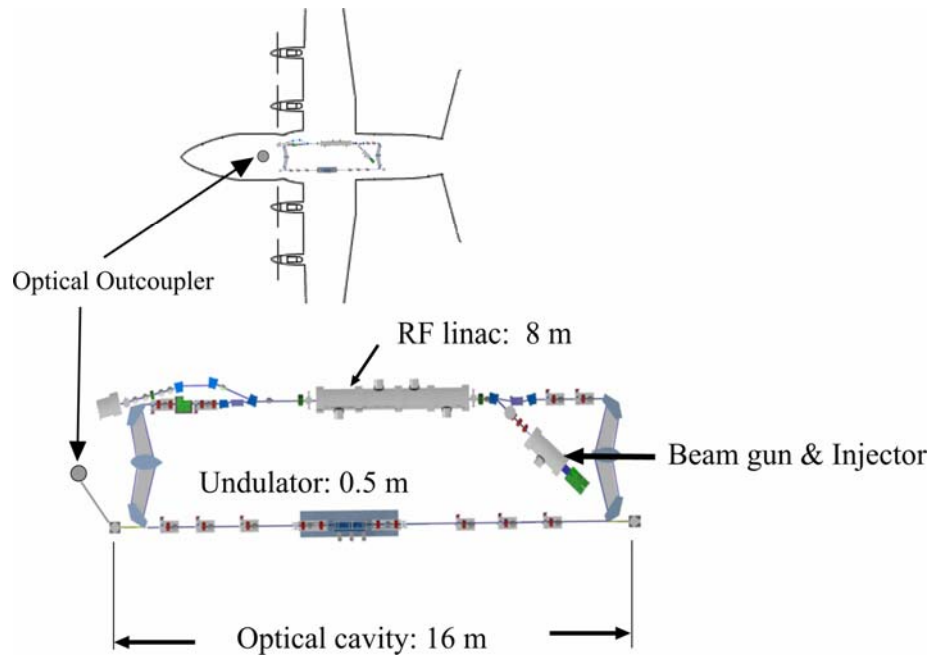


Figure 31. 350 kW Airborne FEL Layout Concept

Note that Figure 31 does not address specific weight issues, but rather simply gives an idea of how the system could fit within a C-130J-30. The beam director would likely be on the underside of the aircraft, although turbulent airflow would need to be considered in the design of such a system.

4. Simulation Results

Simulations were performed to obtain the steady state extraction and output optical power using the parameters listed in Table 6. This program was developed by the Free Electron Research group at NPS, and is used extensively to analyze potential FEL designs and parameters. The numerical results of the simulation are shown in Table 7 below.

Table 7. 350 kW FEL Simulation Results

Output Parameter	Result
Average Optical Power	360 kW
Steady-State Extraction	3%
Peak Intensity at mirrors	140 kW/cm ²

Compared to the 100kW and lower power designs discussed previously in the solid-state laser section, it is clear that an output power of 350 kW is quite significant, and such a system would have greater ability to prosecute a wider variety of ground and airborne targets. A steady-state extraction (percentage of electron beam energy “given” to the optical mode) of 3% was obtained, which is better than typical FEL designs, which generally produce approximately 2% extraction.

Another result of the simulation was the optical mode quality, which is shown in Figure 32 as a three dimensional depiction of transverse optical mode intensity at the outcoupling mirror.

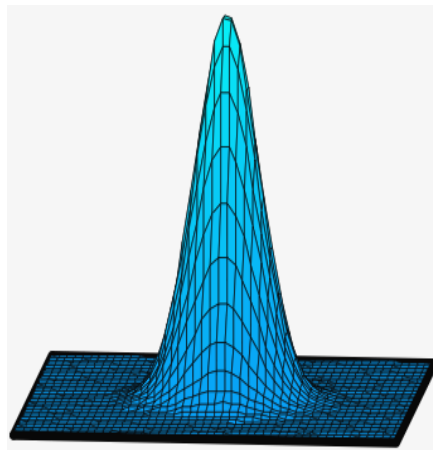


Figure 32. Optical Mode Shape of 350 kW FEL design

Note that the optical mode shown in Figure 32 is composed mainly of the fundamental mode, and is nearly Gaussian in shape. Thus, the value of M^2 is very close to unity.

THIS PAGE INTENTIONALLY LEFT BLANK

IV. FEL THEORY

A. FUNDAMENTAL EQUATIONS

1. Lorentz Equations

The relativistic Lorentz equations governing the motion of the free electrons through the undulator in the presence of an optical field are (in CGS units)

$$\frac{d\gamma}{dt} = \dot{\gamma} = \frac{-e}{mc} (\vec{\beta}_\perp \cdot \vec{E}), \quad (41)$$

$$\frac{d}{dt}(\gamma\vec{\beta}) = \frac{-e}{mc} (\vec{E} + \vec{\beta} \times (\vec{B} + \vec{B}_s)), \quad (42)$$

where

$m \equiv$ electron rest mass ,

$\vec{\beta}_\perp \equiv$ component of $\vec{\beta}$ in the
transverse direction,

$c \equiv$ speed of light in vacuum,

$\gamma \equiv \frac{1}{\sqrt{1-\beta^2}}$ (Lorentz factor),

$e \equiv$ electron charge magnitude,

$\vec{E}_s \equiv$ electric field of optical mode,

$\vec{B} \equiv$ magnetic field of undulator

$\vec{B}_s \equiv$ magnetic field of optical
mode,

$v \equiv$ electron velocity, and $\beta \equiv \frac{v}{c}$

2. Undulator and Optical Field Strengths

The field strengths of the undulator magnetic field and optical fields in a helical undulator are

$$\vec{B} = B(\cos k_0 z, \sin k_0 z, 0) \quad (43)$$

$$\vec{E}_s = E(\cos \psi, -\sin \psi, 0) \quad (44)$$

$$\vec{B}_s = E(\sin \psi, \cos \psi, 0) \quad (45)$$

where

$$\begin{aligned} \vec{B} &\equiv \text{undulator magnetic field,} & z &\equiv \text{longitudinal distance along undulator,} \\ \vec{E}_s &\equiv \text{electric field of optical mode,} & \omega &\equiv \text{angular frequency of optical mode } (\omega = kc), \\ \vec{B}_s &\equiv \text{magnetic field of optical mode,} & t &\equiv \text{time in seconds,} \\ \psi &= kz - \omega t + \phi, & \phi &\equiv \text{optical phase,} \\ k &\equiv \text{wave number of optical mode,} & k_0 &\equiv \frac{2\pi}{\lambda_0}, \\ & & \text{and } \lambda_0 &\equiv \text{undulator period} \end{aligned}$$

B. ELECTRON MOTION IN THE UNDULATOR

The motion of the electron in the helical undulator in the absence of any optical field can be derived using Equation (42) as follows. The magnetic field, whose x and y components vary along the z axis, is

$$\vec{B} = B(\cos k_0 z, \sin k_0 z, 0), \text{ where} \quad (46)$$

$$k_0 = \frac{2\pi}{\lambda_0}.$$

Inserting (46) into the expression $\vec{\beta} \times \vec{B}$ yields

$$\vec{\beta} \times \vec{B} = \hat{x}(-B\beta_z \sin k_0 z) + \hat{y}(B\beta_z \cos k_0 z) + \hat{z}(B\beta_x \sin k_0 z - B\beta_y \cos k_0 z) \quad (47)$$

The x -component of Equation (42) is then

$$\frac{d\beta_x}{dt} = \frac{eB\beta_z}{\gamma mc} \sin k_0 z. \quad (48)$$

and integration gives

$$\beta_x = -\frac{K}{\gamma} \cos k_0 z, \quad (49)$$

where $K = \frac{eB\lambda_0}{2\pi mc^2}$, and the constant of integration is zero representing perfect injection.

Solving for β_{\perp} , the electron velocity (as a fraction of the speed of light) and amplitude of excursions in the transverse (x-y plane) direction yields

$$\beta_{\perp} = -\frac{K}{\gamma}(\cos k_0 z, \sin k_0 z, 0) \quad (50)$$

and, using the approximation $z \approx ct$,

$$\bar{x}_{\perp}(t) = -\frac{K}{\gamma} \frac{\lambda_0}{2\pi} (-\sin \omega_0 t, \cos \omega_0 t, 0) \quad (51)$$

where $\omega_0 = k_0 c$.

As the electron moves longitudinally down the axis of the undulator, the periodic magnetic field causes it to deviate from its straight path, assuming that the injection was sufficiently aligned with the axis of the undulator. The amplitude of this deviation is dependent on both the electron energy and the strength of the magnetic field, as can be seen in Equation 51. The period of these oscillations depends on the spacing of the magnetic fields in the undulator and is given by

$$T = \frac{\lambda_0}{v_z} = \frac{\lambda_0}{\beta_z c} \quad (52)$$

C. ELECTRON MOTION IN THE OPTICAL FIELD

To derive the actual equations of motion, the optical field must be added. A plane wave with helical polarization is assumed, such that

$$\vec{E}_s = E(\cos \psi, -\sin \psi, 0) \quad (53)$$

$$\vec{B}_s = E(\sin \psi, \cos \psi, 0), \quad (54)$$

where \vec{E}_s and \vec{B}_s are the optical magnetic and electric fields. Now,

$$\frac{d}{dt}(\gamma \vec{\beta}_{\perp}) = \frac{-e}{mc} \left[\left(\vec{E}(1 - \beta_z)(\cos \psi, \sin \psi, 0) \right) + \beta_z B(-\sin k_0 z, \cos k_0 z, 0) \right] \quad (55)$$

$$\frac{d}{dt}(\gamma \vec{\beta}_z) = \frac{-e}{mc} \left[E(\beta_x \cos \psi - \beta_y \sin \psi) + B(\beta_x \sin k_0 z - \beta_y \cos k_0 z) \right]. \quad (56)$$

The energy equation (41) can now be written as

$$\dot{\gamma} = \frac{eKE}{\gamma mc} \cos(\zeta + \phi), \quad (57)$$

where the electron phase is $\zeta = (k + k_0)z - \omega t$, and $k \gg k_0$.

To accurately describe the electron motion, the phase acceleration must be obtained using $\dot{\gamma}$ as

$$\beta_z \approx 1 - \frac{1 + K^2}{2\gamma^2} \quad (58)$$

For $\gamma \gg 1$

$$\dot{\zeta} = v = (k + k_0)\beta_z c - \omega = kc \left(1 - \frac{1 + K^2}{2\gamma^2} \right) - \omega \quad (59)$$

is the phase velocity, and thus

$$\ddot{\zeta} = kc \left(\frac{1 + K^2}{2\gamma^2} \right) \left(\frac{2\dot{\gamma}}{\gamma} \right) = \frac{2k_0 eKE}{\gamma^2 m} \cos(\zeta + \phi) \quad (60)$$

Using dimensionless time, defined by $\tau = ct/L$ where L is the undulator length, Equation (60) becomes

$$\frac{d^2 \zeta}{d\tau^2} = \ddot{\zeta} = \dot{\nu} = |a| \cos(\zeta + \phi), \quad (61)$$

where $|a| = (L/c)^2 2k_0 eKE / \gamma^2 m$ is the dimensionless amplitude of the optical field. The dimensionless optical field is a measure of the strength of the E field of the optical mode. Strong fields are defined by a value $a > \pi$, while weak fields are defined as a value $a < \pi$.

The electron phase, ζ , is a measure of the position of the electron with respect to a section of the electron beam one wavelength long. As the light propagates through the undulator, the electrons start at some initial phase, ζ_0 , and fall “behind”, since the light wave travels at a slightly higher speed. This is referred to as the “electron-photon race”, with the rate of change of the phase being the phase velocity, ν . The resonance condition, $\nu = 0$, is given by

$$\lambda = \frac{\lambda_0(1 + K^2)}{2\gamma^2} \quad (62)$$

where λ is the optical wavelength, λ_0 is the undulator magnet spacing, and K is the strength of the magnetic field in the undulator. It turns out that peak extraction efficiency

occurs if the electron “falls back” one wavelength of light over one undulator period, as shown in Figure 33 below.

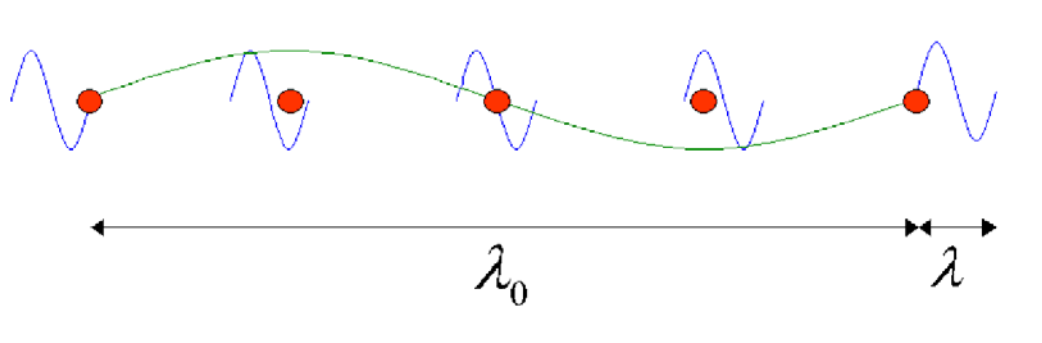


Figure 33. Electron-Photon Race

Here, the electron, shown as a red dot, lags the optical field (blue) so that it arrives -2π from its initial phase after traveling the distance λ_0 (green).

D. PHASE SPACE

The electron beam evolution is most easily described using phase space, which is a plot of the phases of the electron versus its phase velocity $v = d\zeta/d\tau$. The initial electron phase and phase velocity determines the initial position within phase space, and its track through phase space is determined by Equation (61), which is a form of the pendulum equation

$$\ddot{\zeta} = \dot{v} = |a| \cos(\zeta + \phi).$$

The electrons can follow either open or closed orbit paths, depending on initial conditions. These paths are separated by the separatrix, defined as

$$v_s^2 = 2|a|[1 + \sin(\zeta_s + \phi)]. \quad (63)$$

As an analogy to the pendulum, an open orbit path corresponds to a pendulum that swings around without reversing direction, while a closed orbit path corresponds to a pendulum swinging back and forth. Thus, in a closed orbit path (which is the desirable path for the electrons), as the electron phase reaches a maximum, its phase velocity slows

down, then reverses. Figure 33 shows a plot of 20 sample electrons moving through phase space.

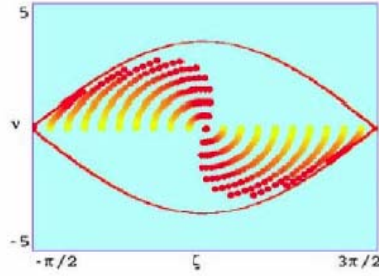


Figure 34. Electrons in Closed Orbit Phase Space Trajectories

In Figure 34, the red line denotes the separatrix. The yellow points indicate the starting position of the electrons. As the electrons move through the undulator, their color changes from yellow to red in the figure. It can be seen that the phases are initially spread out evenly in this case, but after one pass through the undulator, are bunched around $\zeta = \pi/2$. Note that ζ_0 determines the path the electron takes, with v_0 for all of the electrons being zero here. For $\zeta_0 < \pi/2$, $\ddot{\zeta} = \dot{v} > 0$, and thus the phase velocity increases initially showing that the electrons gain energy. This is consistent with the pendulum equation $\ddot{v} = |a_0| \cos(\zeta_0)$, which is positive for values of $\zeta_0 < \pi/2$. For $\zeta_0 > \pi/2$, $\ddot{\zeta} = \dot{v} < 0$, and the electrons lose energy. In this example, there is a clear electron bunching at $\zeta \approx \pi/2$, but no net transfer of energy to the optical wave.

E. THE ELECTRON BEAM IN PHASE SPACE

The electrons in an actual FEL have an optimum initial phase velocity that favors good energy extraction to the optical wave. By Equation (57), it can be seen that $\dot{\gamma} \propto \cos(\zeta)$, meaning that the rate of change of energy of electrons in the beam is determined by the electron phase, and a negative value of $\dot{\gamma}$ describes electrons that are

losing energy to the optical mode. This is the desired situation, and so bunching around $\zeta = \pi$ is the optimum end state.

Figure 35 shows the end state plot of a sample of electrons, after one pass through the undulator. In this case, the electron energy starts slightly off resonance, $\nu_0 > 0$, and there are many more sample electrons than in Figure 34.

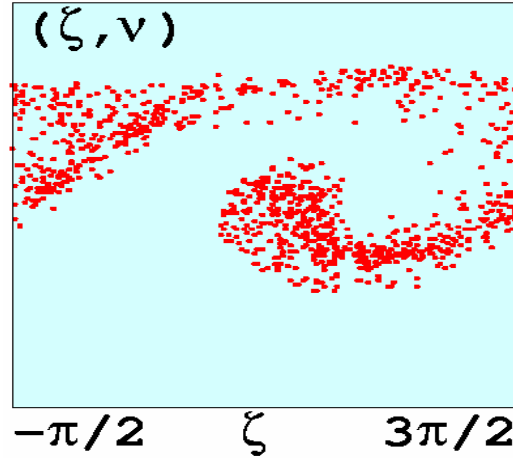


Figure 35. End State Phase Space of Electrons.

Note that in Figure 35, there is some bunching, but not optimum bunching, around $\zeta = \pi$. Some electrons have taken open orbit trajectories, but for the most part, the electrons have stayed inside the separatrix (roughly outlined by the upper band of electrons). Most importantly, more electrons have lost energy than gained it, and this amplifies the optical wave.

THIS PAGE INTENTIONALLY LEFT BLANK

V. FEL UNDULATOR TAPER SIMULATION

A. UNDULATOR TAPER

As the electron travels along the undulator, it loses energy γ , and thus alters the resonance condition,

$$\lambda = \frac{\lambda_0(1 + K^2)}{2\gamma^2}.$$

To compensate for this, the strength of the magnetic field can be adjusted using undulator taper. This alters the pendulum equation governing electron motion such that a new phase acceleration term δ is introduced⁵⁹:

$$\zeta = \delta + |a| \cos(\zeta + \phi), \quad (64)$$

where $\delta = -4\pi N (K^2 / (1 + K^2)) (\Delta K / K)$, and N is the number of undulator periods.

A $\delta > 0$ represents a “positive” taper, where the undulator magnet gap is increased to decrease the field strength. Likewise, a $\delta < 0$ is a “negative” taper, where the field strength is increased. Positive taper is typically the method used, although a negative taper can be effective in some situations. Positive taper is more intuitively logical, since as the electrons lose energy, K must be reduced to compensate and maintain resonance.

B. SIMULATION RESULTS

To find the optimum value of undulator taper for strong field extraction, simulations were performed, varying δ from -4π to 14π . The results of the simulations are shown in Figure 36.

⁵⁹ Colson, W., “Free Electron Lasers” lecture, Naval Postgraduate School, 2004

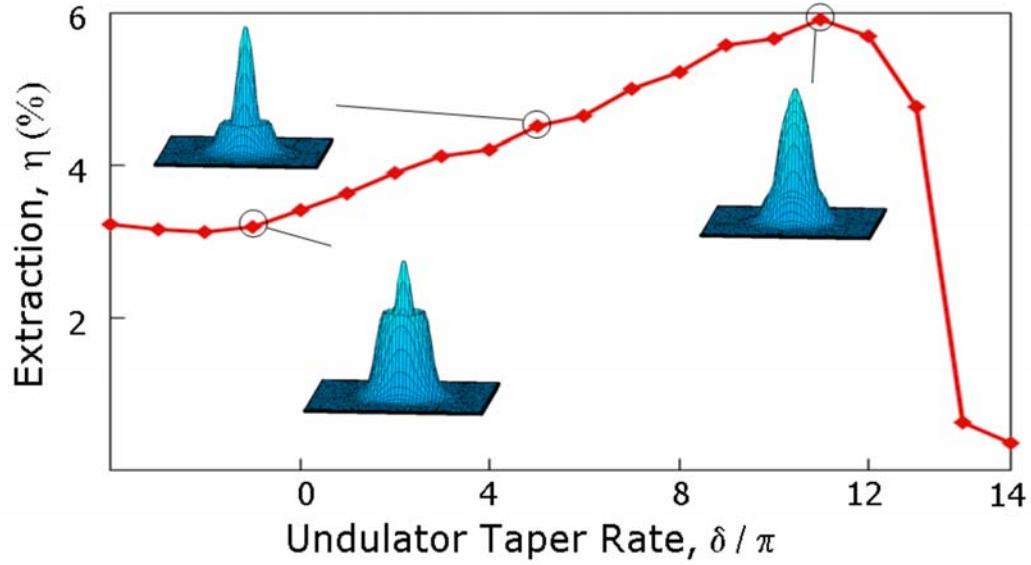


Figure 36. FEL Undulator Taper Rate vs. Strong Field Extraction

It can be seen from Figure 36 that a peak extraction of approximately 6% occurs at $\delta \approx 11\pi$, and thus a positive taper is effective. Also, the optical mode shape seems to improve as the undulator taper rate is increased. The optimum value of $\delta \approx 11\pi$ corresponds to a fractional magnetic field change, $\Delta K / K$, of approximately 10%.

Such improved extraction could enable an FEL to produce more output power, or produce the same power with a reduced average current requirement. The drawback of tapering is that it induces a large energy spread in the electrons. That is, the electrons that aren't optimally bunched end up well outside the separatrix, and this energy spread makes energy recovery through the accelerator more of a challenge. The resulting energy spread found in this case was ~15%⁶⁰ which is within the acceptable limits for recirculation.

⁶⁰ Colson, W. Blau, J. Williams, B., Niles, S., Mansfield, R. "Optical Mode Distortion in a Short Rayleigh Length FEL", presented at the 2004 International FEL conference, Trieste, Italy

LIST OF REFERENCES

1. Townes, C. H., How The Laser Happened, p. 104, Oxford University Press, 1999
2. Svelto, O., Principles of Lasers, 4th ed., Plenum Press, New York and London, 1998
3. Siegman, A., Lasers, University Science Books, Sausalito, California, 1986
4. Kuznetsov, M., Stern, M. Coppeta, J., “Single Transverse Mode Optical Resonators”, *Optics Express*, Vol. 13, No. 1, 10 January 2005
5. Bass, M., Dong, J., “Properties of Diode Laser Pumps for High-Power Solid State Lasers”, *IEEE Journal of Quantum Electronics*, Vol. 41, No.2, February 2005
6. Erwin, S., “Tactical Laser Weapons Still Many Years Away”, *National Defense*, August 2002
7. Koechner, W., Solid State Laser Engineering, 5th ed., Springer, 1999
8. Hall, D. R., Jackson, P. E. The Physics and Technology of Laser Resonators, IOP Publishing, New York, NY, 1989
9. Gapontsev, V., Krupke, W., “Fiber Lasers Grow in Power”, *Laser Focus World*, August 2002
10. Galvanauskas, A., “High Power Fiber Lasers”, *Optics and Photonics News*, July 2004
11. Shirakawa, A., Saitou, T., Sekiguchi, T., Ueda, K., “Coherent addition of fiber lasers by use of a fiber coupler”, *Optics Express*, Vol 10 No. 21, October 2002
12. Mifi, A., Moloney, J., Kouznetsov, D., Schulzgen, A., Jiang, S., Luo, T., Peyghambarian, N., “A Large-Core Compact High-Power Single-Mode Photonic Crystal Fiber Laser”, *IEEE Photonics Technology Letters*, Vol 16 No. 12, December 2004
13. Burris, T. K., “Directed Energy - Worth Analysis and Vehicle Evaluation (DE-WAVE): Military Utility of High-Energy Laser (HEL) Fighter”, AFRL-VA-WP-TR-

- 2003-3082, Lockheed Martin Aeronautics Company, Raytheon Company, Physical Sciences, Inc, Air Force Research Laboratory (AFRL), August 2003
14. Marine Corps Doctrinal Publication 1 (MCDP 1) Warfighting, Headquarters, U.S. Marine Corps, 1997
 15. Joint Publication 1-02 (JP 1-02), U.S. Department of Defense
 16. Marine Aviation Weapons and Tactics Squadron One (MAWTS -1) FAC(A) Handbook, January 2004
 17. Jane's Strategic Weapon Systems, Jane's Information Group, Alexandria, VA, August 2000
 18. TOPGUN Manual, Naval Strike and Air Warfare Center, August 2003
 19. Kessler, C. "Optimized Conventional Power Generation for High Energy Laser Weapons", Presented at the 2004 Solid State and Diode Laser Technology Review Conference
 20. Barnes, P., Rhoads, G. Tolliver, J., Sumption, M., Schmaeman, K., "Compact, Lightweight, Superconducting Power Generators", *IEEE Transactions on Magnetics*, Vol. 41, No. 1, January 2005
 21. Wisken, H., Podeyn, F., Weise, T., "High Energy Density Capacitors for ETC gun applications", *IEEE Transactions on Magnetics*, Vol. 37, No. 1, January 2001
 22. Scheeps, R., Introduction to Laser Diode-Pumped Solid State Lasers, SPIE Press, Bellingham, WA, 2002
 23. NATOPS Flight Manual, Navy Model FA-18E/F 165533 and up aircraft, A1-F18EA-NFM-000, Naval Air Technical Data and Engineering Services Command, San Diego, CA, April 2003
 24. Thornton, S. T., Rex, A., Modern Physics, 2nd ed., Von Hoffman Press, Jefferson City, MO, 2000
 25. Jones-Bey, H., "Livermore Targets Battlefield Environment", *Laser Focus World*, December 2003

26. Wang, Y. "Heat Dissipation in Kilowatt Fiber Power Amplifiers", *IEEE Journal of Quantum Electronics*, Vol. 40, No. 6, June 2004
27. Limpert, J., Deguil-Robin, N., Manek-Honninger, I., Salin, F., Roser, F., Liem, A., Schreiber, T., Nolte, S., Zellmaier, H., Tunnermann, A., Broeng, J. , Petersson, A., Jakobsen, C., "High-power rod-type photonic crystal fiber laser", *Optics Express*, Vol. 13, No. 4, 21 February 2005
28. Zuev, V. E. Laser Beams in the Atmosphere, Plenum Publishing, New York, NY, 1982

THIS PAGE INTENTIONALLY LEFT BLANK

INITIAL DISTRIBUTION LIST

1. Defense Technical Information Center
Ft. Belvoir, Virginia
2. Dudley Knox Library
Naval Postgraduate School
Monterey, California
3. Marine Corps Representative
Naval Postgraduate School
Monterey, California
4. Director, Training and Education
MCCDC, Code C46
Quantico, Virginia
5. Director, Marine Corps Research Center
MCCDC, Code C40RC
Quantico, Virginia
6. Marine Corps Tactical Systems Support Activity (Attn: Operations Officer)
Camp Pendleton, CA
7. Dr. Roy Whitney
Jefferson Laboratory
Newport News, Virginia
8. Warfare Analysis Department
NAVAIR
Patuxent River, Maryland
9. Ms. Michelle Creedon
Northrop-Grumman Space Technology
Los Angeles, California
10. Mr. William R. Long
NAVAIR
China Lake, California
11. Ms. Karla Meyn
AIRTEVRON Nine
China Lake, California

12. Dr. William B. Colson
Naval Postgraduate School
Monterey, California
13. Dr. Robert L. Armstead
Naval Postgraduate School
Monterey, California
14. Col Lewis Watt, USMC (Ret)
RLW, Inc.
State College, Pennsylvania
15. Major Michael Dehner, USMC
NAVAIR
Patuxent River, Maryland